Pc1–Pc2 waves and energetic particle precipitation during and after magnetic storms: Superposed epoch analysis and case studies

M. J. Engebretson,[1] M. R. Lessard,[2] J. Bortnik,[3] J. C. Green,[4] R. B. Horne,[5] D. L. Detrick,[6] A. T. Weatherwax,[7] J. Manninen,[8] N. J. Petit,[9] J. L. Posch,[1] and M. C. Rose[5]

Received 22 February 2007; revised 30 July 2007; accepted 24 September 2007; published 24 January 2008.

[1] Magnetic pulsations in the Pc1–Pc2 frequency range (0.1–5 Hz) are often observed on the ground and in the Earth's magnetosphere during the aftermath of geomagnetic storms. Numerous studies have suggested that they may play a role in reducing the fluxes of energetic ions in the ring current; more recent studies suggest they may interact parasitically with radiation belt electrons as well. We report here on observations during 2005 from search coil magnetometers and riometers installed at three Antarctic stations, Halley (−61.84° magnetic latitude, MLAT), South Pole (−74.18° MLAT), and McMurdo (−79.96° MLAT), and from energetic ion detectors on the NOAA Polar-orbiting Operational Environment Satellites (POES). A superposed epoch analysis based on 13 magnetic storms between April and September 2005 as well as case studies confirm several earlier studies that show that narrowband Pc1–Pc2 waves are rarely if ever observed on the ground during the main and early recovery phases of magnetic storms. However, intense broadband Pi1–Pi2 ULF noise, accompanied by strong riometer absorption signatures, does occur during these times. As storm recovery progresses, the occurrence of Pc1–Pc2 waves increases, at first in the daytime and especially afternoon sectors but at essentially all local times later in the recovery phase (typically by days 3 or 4). During the early storm recovery phase the propagation of Pc1–Pc2 waves through the ionospheric waveguide to higher latitudes was more severely attenuated. These observations are consistent with suggestions that Pc1–Pc2 waves occurring during the early recovery phase of magnetic storms are generated in association with plasmaspheric plumes in the noon-to-dusk sector, and these observations provide additional evidence that the propagation of waves to ground stations is inhibited during the early phases of such storms. Analysis of 30- to 250-keV proton data from four POES satellites during the 24–27 August and 18–19 July 2005 storm intervals showed that the location of the inner edge of the ring current matched well with the plasmapause model of O'Brien and Moldwin (2003). However, the POES data showed no evidence of the consequences of electromagnetic ion cyclotron waves (localized proton precipitation) during main and early recovery phase. During later stages of the recovery phase, when such precipitation was observed, it was coincident with intense wave events at Halley, and it occurred at L shells near or up to 1 R_E outside the modeled plasmapause but well equatorward of the isotropy boundary.

Citation: Engebretson, M. J., et al. (2008), Pc1–Pc2 waves and energetic particle precipitation during and after magnetic storms: Superposed epoch analysis and case studies, *J. Geophys. Res.*, *113*, A01211, doi:10.1029/2007JA012362.

1. Introduction

[2] Since early in the space age, several studies have documented an association between magnetic storms

[1]Department of Physics, Augsburg College, Minneapolis, Minnesota, USA.
[2]Space Science Center and Department of Physics, University of New Hampshire, Durham, New Hampshire, USA.
[3]Department of Atmospheric and Oceanic Sciences, University of California, Los Angeles, California, USA.
[4]NOAA Space Environment Center, Boulder, Colorado, USA.
[5]British Antarctic Survey, Cambridge, U.K.
[6]Institute for Physical Science and Technology, University of Maryland, College Park, Maryland, USA.
[7]Department of Physics, Siena College, Loudonville, New York, USA.
[8]Sodankylä Geophysical Observatory, Sodankyla, Finland.
[9]Department of Computer Science, Augsburg College, Minneapolis, Minnesota, USA.

0148-0227/08/2007JA012362$09.00

(especially their aftermath) and an increase in the occurrence of electromagnetic waves in the Pc1–Pc2 frequency band (0.1–5.0 Hz) in the Earth's magnetosphere. An association between these waves and the aftermath of geomagnetic storms was observed in early work by *Wentworth* [1964], *Campbell* [1967], and *Heacock and Kivinen* [1972]; each study found that wave occurrence was largest several days after storm onset. These waves, now identified as electromagnetic ion cyclotron (EMIC) waves, are understood to be one of several mechanisms in addition to charge exchange that can contribute to the decay of the storm-time ring current [*Kozyra et al.*, 1997; *Jordanova et al.*, 2001]. A resurgence of interest in radiation belt electrons and the geomagnetic storms that often cause their fluxes to increase has again focused attention on these waves, in part because they have also been associated with the rapid loss of radiation belt electrons [e.g., *Summers and Thorne*, 2003; *Meredith et al.*, 2003].

[3] Wave-particle interactions in the ring current were reviewed by *Daglis et al.* [1999], and more recently those interactions relevant to the loss of radiation belt electrons were reviewed by *Thorne et al.* [2005]. Since EMIC waves can be driven by unstable (anisotropic) distributions of protons [*Cornwall*, 1965; *Kennel and Petschek*, 1966; *Kozyra et al.*, 1997], the amplitude of the waves is likely correlated with increases in the ring current, and would lead to precipitation of ring current ions.

[4] Both early and recent theoretical studies have demonstrated that EMIC waves should also be an effective means of loss of >1 MeV electrons from the radiation belts in regions of increased magnetospheric particle density [e.g., *Lyons et al.*, 1972; *Thorne et al.*, 1973; *Summers and Thorne*, 2003; *Albert*, 2003]. Pitch angle diffusion rate calculations by *Summers and Thorne* [2003] and *Albert* [2003] showed that waves with frequency less than the He^+ and H^+ gyrofrequencies are very effective in scattering relativistic electrons into the loss cone via a parasitic interaction. The relative contributions to electron loss during the main phase by wave-particle interactions and by transport processes, however, are as yet unknown. EMIC waves may also contribute to loss of these electrons on longer timescales as the ring current decays. However, since the loss cone is very small for $L > 4$ in the equatorial region it is very difficult to link electron precipitation with EMIC observations in the outer magnetosphere.

[5] An additional complication is that the propagation of EMIC waves to the ionosphere is strongly affected by the presence of heavy ions (He^+ and O^+). Ray tracing studies have shown that waves with frequency below the heaviest ion gyrofrequency can propagate to the ionosphere and transmit energy to the ground [*Rauch and Roux*, 1982; *Horne and Thorne*, 1993, 1994]. Those with a higher frequency are reflected at midlatitudes at the location on the magnetospheric field line where the wave frequency matches the local bi-ion frequency. Such waves can, however, propagate to the ionosphere if the concentration of heavy ions is low [*Johnson and Cheng*, 1999]; such waves reach the ground in about 50% of the cases observed [*Perraut et al.*, 1984].

[6] In this study we combine ground-based magnetometer observations of Pc1–Pc2 waves with simultaneous riometer observations of overhead energetic electron precipitation, and with observations of precipitating 30- to 250-keV protons from four Polar-orbiting Operational Environment Satellites (POES). In a follow-up study we examine the fluxes of precipitating radiation belt electrons observed by the POES and SAMPEX satellites in order to seek evidence of the parasitic interaction of Pc1–Pc2 waves on outer radiation belt electron populations.

[7] Although some of the patterns reported here in ground-based observations of ULF wave occurrence and frequency have been noted earlier, the additional focus in this study on broadband ULF noise and its association with riometer absorption has been lacking in most earlier studies. The comparison of both of these data sets with precipitation data from low-altitude satellites provides additional information on the relation between ULF activity, both EMIC waves and broadband ULF noise, and fluxes of ring current protons.

2. Data Set

[8] A three-axis search coil magnetometer was deployed at the Halley research station near the coast of Antarctica (at subauroral latitudes, $L = 4.56$) in late February 2005. Halley joins an existing high-latitude array of search coil magnetometers in Antarctica, including South Pole (at cusp latitudes, $L \sim 13$), and McMurdo (in the polar cap), each of which measures the rate of change of the ambient vector geomagnetic field, dB/dt, at a rate of 10 Hz, and several automated geophysical observatories (AGOs) that typically make measurements at 2 Hz. At each station, data are recorded in local geomagnetic coordinates with X northward, Y eastward, and Z oriented along the local field [*Taylor et al.*, 1975; *Engebretson et al.*, 1997].

[9] Figure 1 shows the location of Halley, South Pole Station (SP), and McMurdo (MC) in Antarctica, and the geographic and geomagnetic coordinates of these stations are listed in Table 1. Halley and South Pole are situated at similar magnetic longitudes.

[10] Four La Jolla 30-MHz riometers are deployed at Halley at 45° elevation in each invariant magnetic cardinal direction to provide spatial discrimination with 1 s resolution [*Dudeney et al.*, 1995, 1997]. The 38.2-MHz riometer located at South Pole Station employed a zenith-centered dipole antenna with a half-power beam width of about 60° [*Chivers*, 1975], and was also sampled at 1-s resolution. Riometer absorption is dependent on the inverse square of the RF wave frequency, so in order to intercompare the overhead precipitation level, we have converted the South Pole absorption values into equivalent values at 30 MHz.

[11] The POES satellites, in Sun-synchronous 98.6° inclination orbits at ~833 km altitude, measure precipitating protons with energies from 30 keV to over 200 MeV using the Medium Energy Proton and Electron Detector (MEPED) [*Evans and Greer*, 2000]. Four satellites, POES 15, 16, 17, and 18 were in operation during the intervals presented here.

[12] This study uses data from a ~6 month period during 2005 (5 April to 17 September) during which a succession of magnetic storms occurred, as indicated in Figure 2. The upper plot of Figure 2 is a survey plot of SAMPEX 2- to 6-MeV radiation belt electron fluxes from 31 March through 17 September 2005 (days 05090–05260), courtesy of

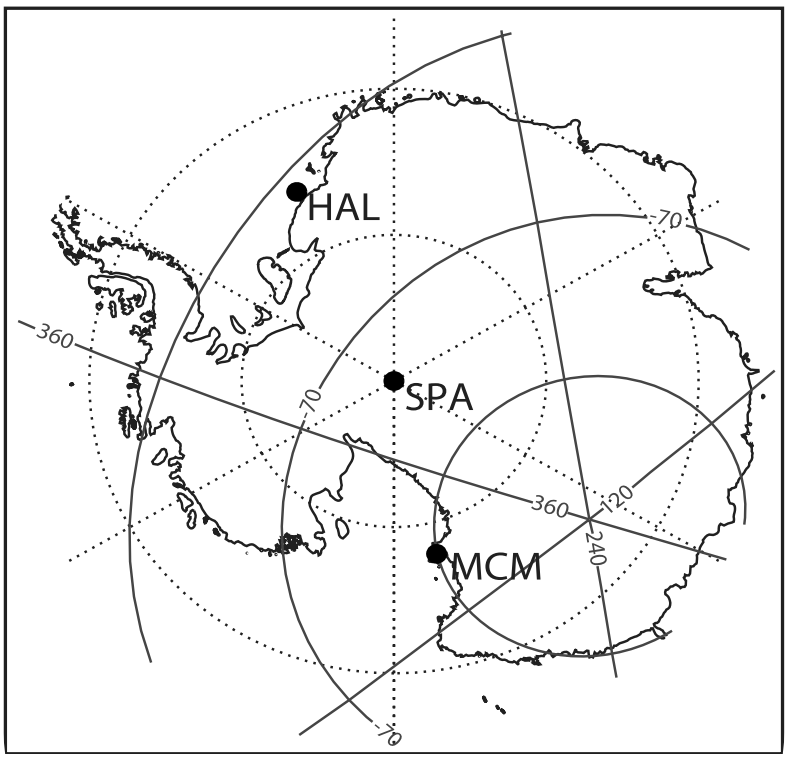

Figure 1. Map of Antarctica showing the locations of Halley (HAL), South Pole (SPA), and McMurdo (MCM). Dotted lines indicate geographic coordinates, and solid lines indicate geomagnetic coordinates.

S. Kanekal, and the lower plot is a plot of the provisional *Dst* index for this same interval. Table 2 lists the days included in this analysis, and also the time of minimum *Dst* for each storm, which ranged in intensity from −53 to −263 nT. Data dropouts during May and June related to an electrical grounding problem (since repaired) are responsible for all but one of the missing days; high noise levels due to strong surface winds caused broadband interference on 14 August.

3. Case Studies

[13] Figures 3, 4, and 5 present stacked 0–2.5 Hz Fourier spectrograms of search coil data from Halley, South Pole, and McMurdo and riometer data from Halley and South Pole for six selected days. Figures 3 and 4 include the onset and early recovery period of the most intense magnetic storm occurring during this interval (minimum *Dst* = −216), beginning on 24 August 2005. Figure 5 shows the first two days of the weaker 18 July 2005 storm (minimum *Dst* = −76). Differencing is used in these spectrograms of magnetic field data to facilitate display of a wide range of spectral power by removing the f^{-2} falloff in spectral power, but without loss of information about the background signal. *Takahashi et al.* [1990] give a quantitative relationship between spectral power calculated from differenced and undifferenced data. Differencing of search coil data, which is already a measure of dB/dt, was done in order to make the Pc1–Pc2 signals more prominent in comparison with the broadband (Pi1) and lower-frequency ULF signals that are often observed at these stations. Wave power is color-coded according to the color bar at the right. Riometer absorption plots similarly cover the entire day, and are plotted with a uniform scale of 0 to 4 dB.

[14] The sixth, seventh, and eighth panels of Figures 3–5 show, respectively, the earthward component of the solar wind velocity (|Vx|), the solar wind dynamic pressure (P_{sw}), and the north-south (Bz) component of the interplanetary magnetic field (IMF), as measured by the ACE spacecraft at the upstream L1 point. Data in these panels have been time-shifted to compensate for the delay time between ACE and the Earth's magnetosphere.

Table 1. Coordinates of the Search Coil Magnetometer Sites Used in This Study[a]

	Geographic		Geomagnetic			MLT of Local Noon,
Station	Latitude	E Longitude	Latitude	E Longitude	*L*	UT
Halley	−75.50	333.40	−61.84	29.31	4.56	1444
South Pole	−90.00	0.0	−74.18	18.51	13.66	1537
McMurdo	−77.85	166.67	−79.96	326.54	undefined	1901

[a]Geomagnetic coordinates and values of *L* and magnetic local time (MLT) of noon are based on algorithms at the Space Physics Data Facility/Modelweb Web site, http://modelweb.gsfc.nasa.gov/models/cgm/cgm.html, for epoch 2005, assuming an altitude of 100 km.

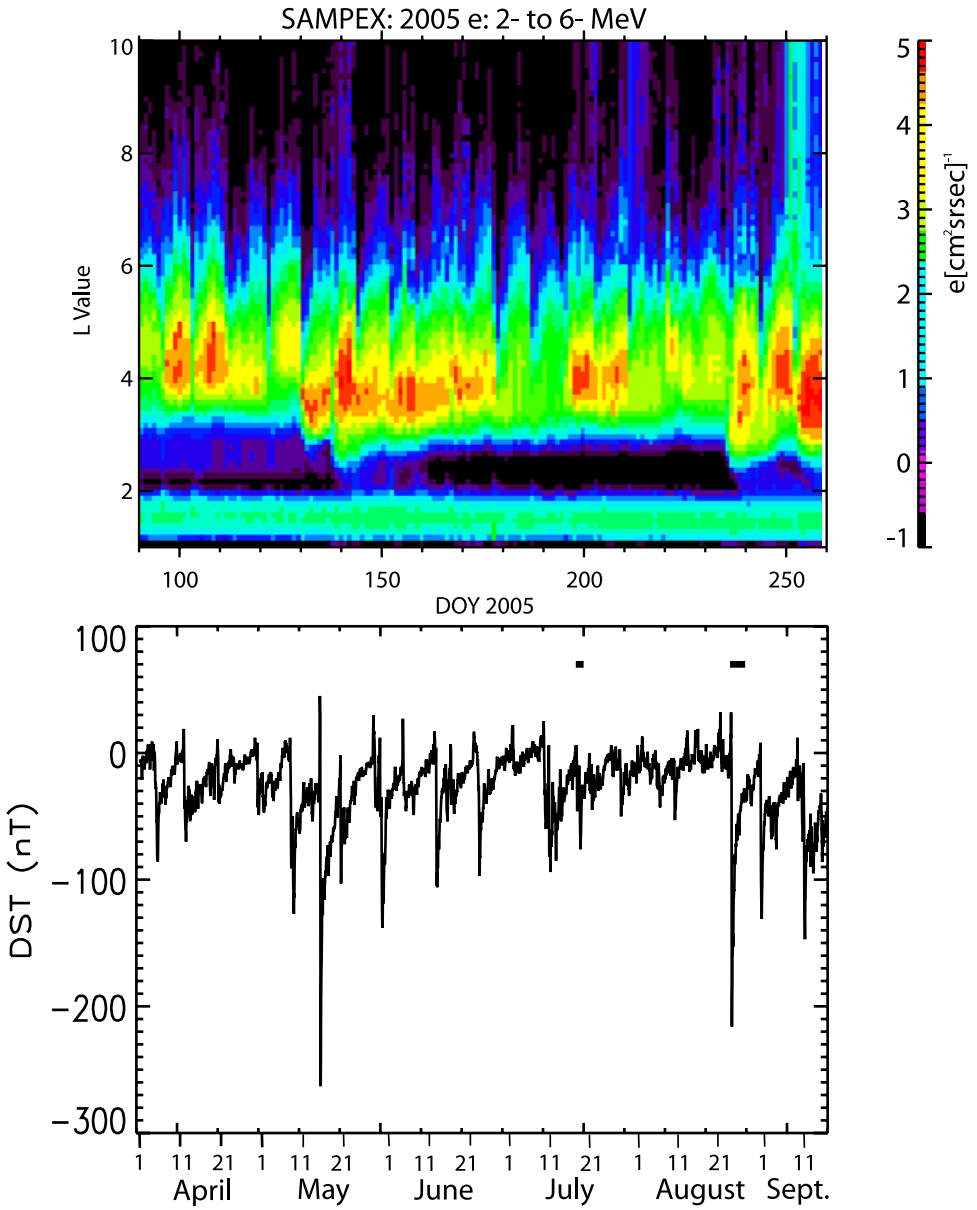

Figure 2. SAMPEX survey plot of 2- to 6-MeV radiation belt electron fluxes (courtesy of S. Kanekal, 2006) and plot of the provisional *Dst* index, during the interval of this study, days 90–260, 2005. The thick short lines in the lower panel indicate the two storm intervals selected for detailed study.

Table 2. Days of Storm Onset and Recovery During 2005 Included in the Superposed Epoch Analysis[a]

Onset	D1	D2	D3	D4	D5	D6	Min *Dst*, nT	UT of Min, h
5 Apr	6 Apr	7 Apr	8 Apr	9 Apr	10 Apr	11 Apr	−85	0500–0700
12 Apr	13 Apr	14 Apr	15 Apr	16 Apr	17 Apr	18 Apr	−70	0500–0600
			18 May	19 May			−263	0800–0900
20 May	21 May	22 May	23 May	24 May	25 May	26 May	−103	0800–0900
30 May	31 May	1 Jun	2 Jun	3 Jun			−138	1300–1400
				17 Jun	18 Jun		−106	0000–0100
23 Jun	24 Jun	25 Jun	26 Jun	27 Jun	28 Jun	29 Jun	−97	1000–1100
10 Jul	11 Jul	12 Jul	13 Jul	14 Jul	15 Jul	16 Jul	−94	2000–2100
18 Jul	19 Jul	20 Jul	21 Jul	22 Jul	23 Jul	24 Jul	−76	0600–0700
10 Aug	11 Aug	12 Aug	13 Aug		15 Aug	16 Aug	−53	1100–1200
24 Aug	25 Aug	26 Aug	27 Aug	28 Aug	29 Aug	30 Aug	−216	1100–1200
31 Aug	1 Sep	2 Sep	3 Sep	4 Sep	5 Sep	6 Sep	−131	1900–2000
11 Sep	12 Sep	13 Sep	14 Sep	15 Sep	16 Sep	17 Sep	−123	1000–1100

[a]The two columns at the far right show the minimum *Dst* value at storm onset and the hour(s) during which this value occurred.

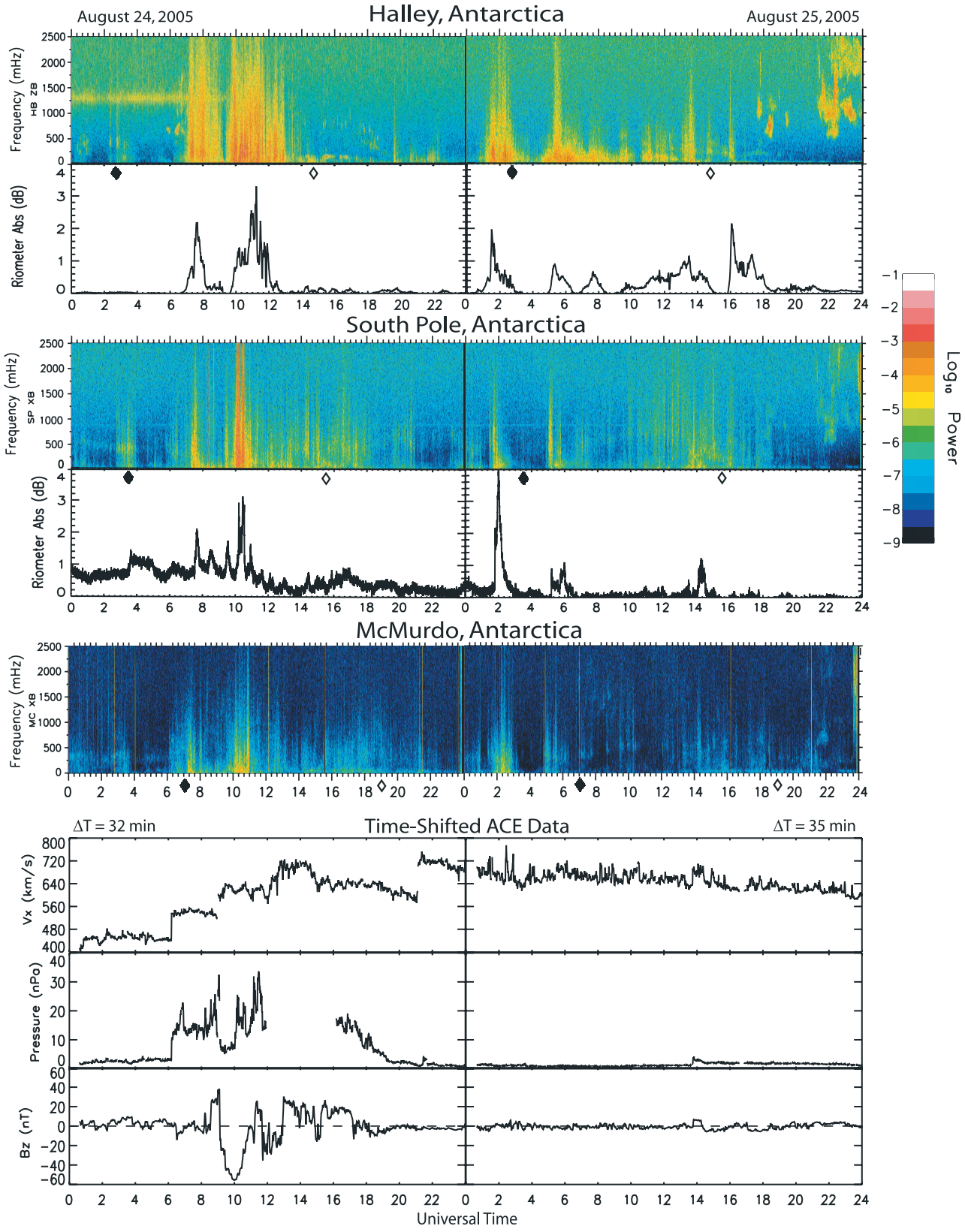

Figure 3. Stacked daily 0- to 2.5-Hz Fourier spectrograms of differenced search coil magnetometer data from Halley, South Pole, and McMurdo, Antarctica (first, third, and fifth panels, respectively) and plots of riometer absorption (second and fourth panels) from Halley and South Pole, for 24 and 25 August 2005. Local midnight and noon are indicated by solid and open diamonds, respectively. The sixth, seventh, and eighth panels show time-shifted solar wind velocity, solar wind pressure, and interplanetary magnetic field (IMF) Bz data measured by the ACE spacecraft.

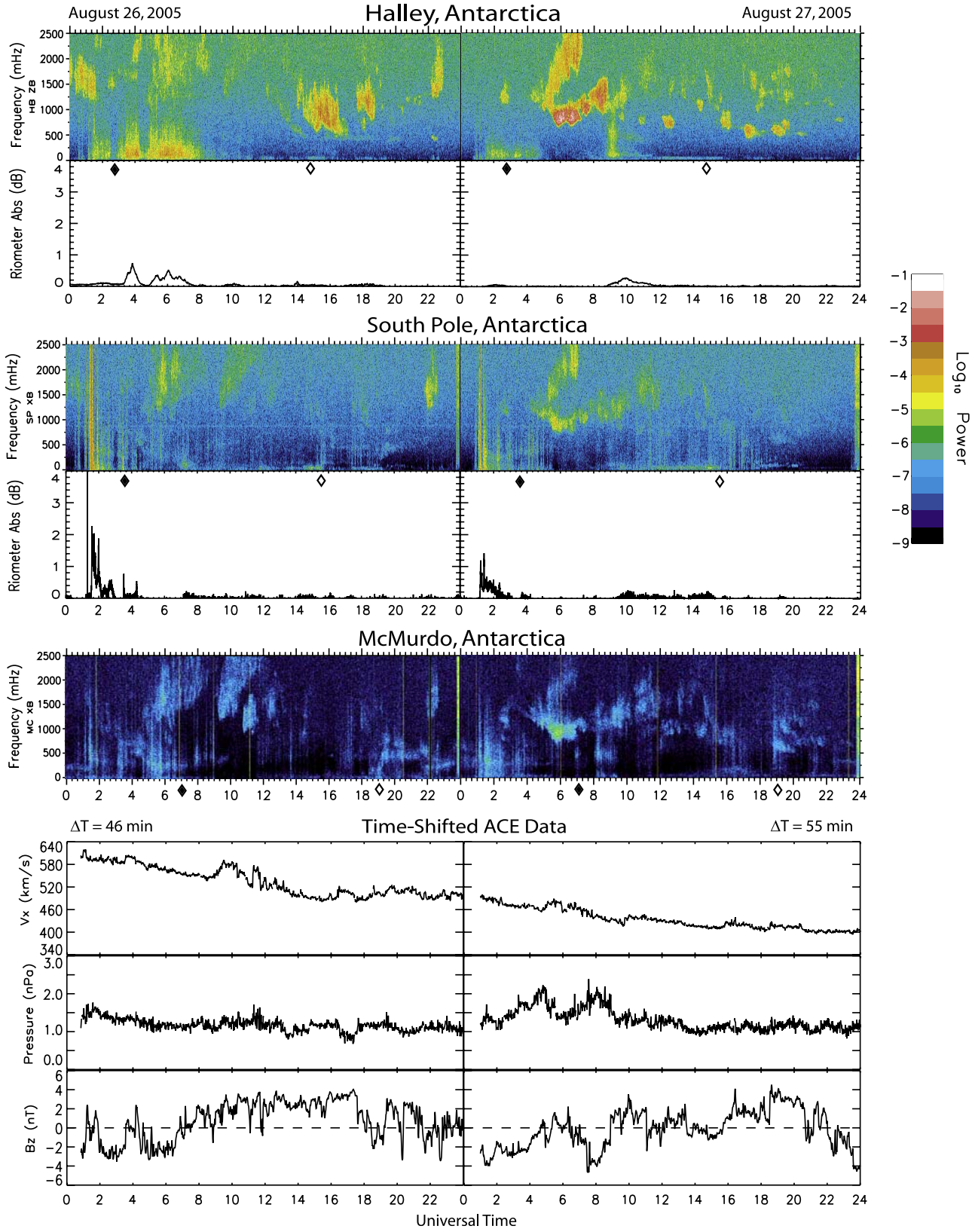

Figure 4. Stacked daily 0- to 2.5-Hz Fourier spectrograms of differenced search coil magnetometer data and plots of riometer absorption and IMF–solar wind data, as in Figure 3, for 26 and 27 August 2005.

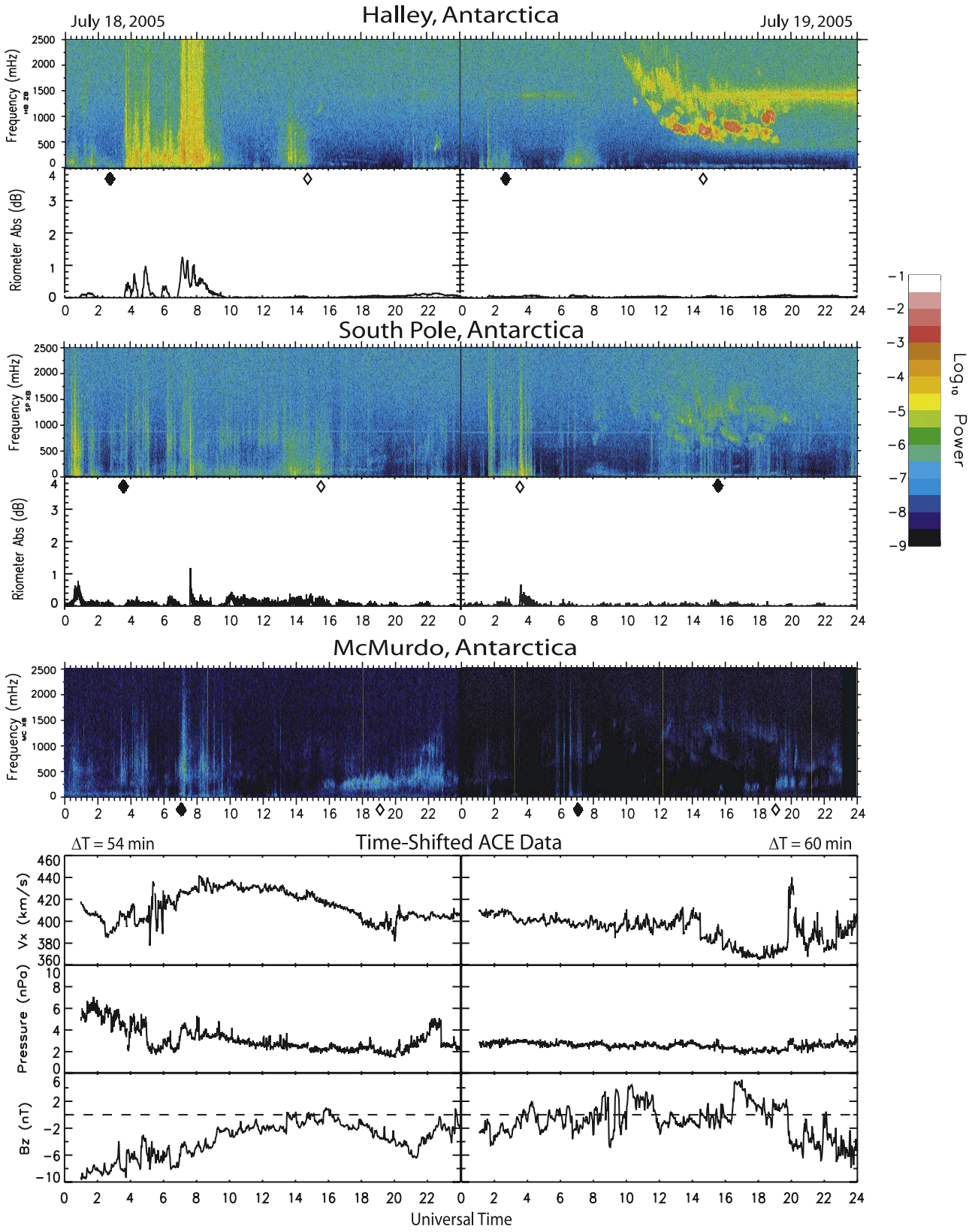

Figure 5. Stacked daily 0- to 2.5-Hz Fourier spectrograms of differenced search coil magnetometer data and plots of riometer absorption and IMF–solar wind data, as in Figure 3, for 18 and 19 July 2005.

3.1. 24–27 August 2005

[15] The magnetic storm that began on 24 August was stimulated by a complicated rise in both solar wind density and velocity. A sudden jump in P_{sw} from ~3 to ~12 nPa simultaneous with an increase in V_{sw} from 450 to 540 km/s is evident near 0620 UT 24 August, in the left-hand panel of Figure 3. A sharp decrease in P_{sw} near 0910 UT was followed by an even larger increase near 1010 UT. By the time V_{sw} reached its maximum value near 720 km/s at 2120 UT, P_{sw} had diminished to 2 nPa, below its prestorm value. IMF Bz reached a value of ~−52 nT at 1010 UT, and exhibited large oscillations for ~7 h before returning to values above −5 nT for the remainder of the day. V_{sw} declined gradually during the three subsequent days, remaining above 600 km/s during 25 August but reaching 400 km/s by the end of 27 August.

[16] Two short bursts of Pc1 wave activity occurred at Halley near 0.6 Hz between 0530 and 0630 UT on 24 August (left-hand panels of Figure 3), shortly before the increased P_{sw} and V_{sw} impacted the Earth's magnetosphere. After storm onset, no other Pc1–Pc2 signals were observed during this day. (The signal at Halley near 1.3 Hz from 0000 to 0900 UT is an artifact of high surface winds at Halley, and is hence of no interest for this study.) No narrowband wave activity was evident at any time on this day at the two higher-latitude stations, South Pole and McMurdo.

[17] Intense broadband noise appeared in the Halley search coil spectrogram from 0700 to 1300 UT, the times when the most intense solar wind pressure impacted the Earth's magnetosphere, and similar broadband noise intensified at South Pole and McMurdo during this same interval. Comparison of the intensity of the broadband wave signals with the overhead riometer absorption at Halley indicates good temporal agreement throughout most of the day; only after 2200 UT did the peaks not match up. Riometer absorption at both South Pole (fourth panel of Figure 3) and McMurdo (not shown) was dominated by a strong solar proton event that began many hours before storm onset. At South Pole, agreement between broadband wave activity and peaks in riometer absorption was quite good from 0730 to 1800 UT, but again poor thereafter. Riometer absorption at McMurdo from 0730 to 0830 and from 1000 to 1100 UT (during which time it exceeded 4 dB) was correlated with increases in overhead optical auroral emissions (not shown), and was in good temporal agreement with intensifications of ULF wave activity shown in the McMurdo search coil spectrogram in Figure 3.

[18] During the first day after the storm onset, 25 August (right-hand panels of Figure 3), the ULF spectrograms were again dominated by broadband noise until late in the day. The riometer signals during this interval were somewhat less intense but of longer duration at Halley, and reached higher substorm-related peak values at South Pole near 0200 UT this day than on the previous day. A spike in ULF power and riometer absorption beginning at 1340 UT most likely occurred in response to the pulse in P_{sw} and IMF Bz evident at this time in the ACE data. The McMurdo riometer data (not shown) was still dominated by solar protons, except near 0200 UT.

[19] Three bursts of moderate to intense Pc1 wave activity appeared at Halley from 1730 to 1930 UT, but only faint traces of wave power appeared simultaneously at South Pole. No wave power above background could be seen at McMurdo. More sustained moderate to intense Pc1 wave activity appeared from 2120 UT through the end of the day at Halley, and weak signals of the lowest frequency of these waves appeared simultaneously at South Pole and McMurdo.

[20] Weaker riometer absorption and broadband ULF signals appeared during the early hours (local nighttime) of the second recovery day 26 August (left-hand panels of Figure 4) at all three stations. Intervals of increased riometer absorption at Halley (before 0800 UT) may well be correlated with roughly simultaneous intervals of negative IMF Bz.

[21] Pc1 activity occurred sporadically throughout this day as well. Strong 1.3–2.0 Hz Pc1 activity appeared at Halley from 0000 to 0150 UT, but very little power in this frequency range was evident at South Pole, and none at McMurdo. Other Pc1 activity above 1 Hz appeared at Halley intermittently from 0140 to 0820 UT, even during times of intense lower-frequency broadband ULF noise. While most of this Pc1 activity did not appear at South Pole or McMurdo, the wave activity that occurred between 0600 and 0800 UT did. Waves with rising frequency, resembling a typical IPDP event (intervals of pulsations of diminishing period [*Hayakawa et al.*, 1992]) but at higher frequency, appeared at all three stations, with intensity roughly comparable at Halley and South Pole but considerably weaker at McMurdo. Similar rising-frequency waves from 1040 to 1300 UT were most evident at McMurdo, were slightly more intense at South Pole, but were not evident at Halley. This suggests they were generated at a longitude somewhat farther from Halley, and propagated poleward through the ionosphere (as did all the other waves) to the higher-latitude stations.

[22] Intense 0.5–1.5 Hz wave activity appeared at Halley from 1400 to 1700 UT and from 1730 to 1830 UT; both intervals corresponded to times of increased P_{sw}. Only very weak traces of these waves were evident at South Pole, and none at McMurdo. Riometer absorption increased at Halley during both of these wave intervals, but was negligible at South Pole and McMurdo. A later burst of 1.3–2.4 Hz wave activity from 2200 to 2300 UT, however, appeared clearly at both South Pole and McMurdo. No riometer absorption was evident at any of the three stations during this wave burst.

[23] Similar data for 27 August, day 3 of the recovery phase, are shown in the right-hand panels of Figure 4. Intervals of southward IMF Bz again correlated fairly well with (weaker) riometer absorption signatures at Halley early in the day. As on earlier days, riometer absorption at Halley and South Pole coincided with broadband ULF noise, but again on this day such noise did not prevent the detection of Pc1 waves during nighttime at either station.

[24] A burst of Pc1 activity appeared at Halley and more weakly at South Pole and McMurdo between 0230 and 0300 UT. Intense Pc1 activity beginning near 0500 UT split into two frequency bands, the higher rising rapidly to a maximum of 2.8 Hz (not shown) at 0640 UT and ending abruptly at 0715 UT, the lower ranging from 0.6 to 1.0 Hz near 0600 UT and rising more slowly (to 1.6 Hz) and also ending abruptly, at 0850 UT. Signals from both bands appeared clearly at South Pole and McMurdo. Continued activity in the lower band past 0850 UT suggests that again

the higher-latitude stations were receiving ionospherically ducted activity generated at longitudes no longer near Halley. Pc1 activity after 1000 UT at Halley was more bursty, with intense activity below 1 Hz and weaker activity from 1 to 2 Hz. Weak signals from some but not all of these wave bursts also appeared at South Pole and McMurdo. Similar wave activity appeared on day 4 of the recovery phase (28 August, not shown), with high-frequency Pc1 activity during local nighttime hours (up to 3.2 Hz) but with exclusively lower-frequency activity during the daytime (all below 0.8 Hz). Riometer data from Halley were also weaker than during 27 August.

[25] The fact that the ULF spectral patterns usually appear identical (except for amplitude) for each wave event at all three stations strongly suggests that each event is generated in a localized flux tube or region of flux tubes, and propagates along them to the Antarctic ionosphere. In this region, some of the wave power is transmitted to the ground, and some is ducted long distances horizontally through the ionospheric F region duct [*Manchester*, 1966; *Tepley and Landshoff*, 1966; *Greifinger and Greifinger*, 1968; *Fujita*, 1987; *Fujita and Tamao*, 1988a, 1988b]. We point out that using ground-based data from such widely spaced stations alone, we cannot determine whether any of these waves occurred on field lines "overhead" of Halley, in which case they could propagate down the field lines directly to that station, or whether they have been ducted some modest distance horizontally through the ionosphere. The higher intensity of the waves at Halley relative to those at South Pole and McMurdo simply suggests that the waves were generated on flux tubes much nearer to Halley. Poor wave propagation to larger L shells is even consistent with the possibility that Pc1 waves occurred at L shells below Halley during the first two days of the storm. In section 5 we address this difficulty using in situ observations of precipitating protons by the POES satellites. However, POES data (Figure 9 below) does not show isolated regions of proton precipitation at low L in the Halley longitude sector during these first two days, either.

[26] We can also comment briefly on the temporal structure of the Pc1–Pc2 waves observed during these four days. The waves before storm onset on 24 August were structured (had "pearl" structure). On 25 August the waves between 1800 and 2200 UT had considerable temporal structure, but it was not repetitive. Between 2200 and 2400 UT, however, the waves were pearls. Many of the waves on 26 August were pearls: between 0100 and 0430 UT and from 1430 to 2300 UT. All of the waves on 27 August were pearls, as well.

3.2. 18–19 July 2005

[27] The magnetic storm that occurred during this interval was quite effective in energizing the outer radiation belt (cf. Figure 2), but was associated with only modest V_{sw} values, which peaked near 510 km/s early on 17 July. Two weak *Dst* minima on 17 June were followed by an interval of increased P_{sw} and sustained large negative Bz values from late 17 July through early 18 July (Figure 5).

[28] Broadband noise dominated the Halley search coil data early on 18 July with the most intense activity (from 0330 to 0830 UT) spanning the time of minimum *Dst* (0600–0700 UT). Peaks in riometer absorption again occurred in good temporal agreement with broadband ULF signatures. Only two very weak intervals of Pc1–Pc2 wave activity were observed at Halley on this day, from 1 to 1.3 Hz near 1530 UT and from 0.3 to 0.6 Hz near 2230 UT.

[29] Weaker broadband ULF noise was observed at South Pole and McMurdo throughout much of the day. The South Pole ULF noise was again temporally associated with local riometer absorption but not with features observed at Halley. Late in the day, however, narrowband Pc1–Pc2 signals appeared at McMurdo, in the polar cap, near local noon.

[30] Observations on 19 July 2005, day 1 of the recovery phase, are shown in the right-hand panels of Figure 5. Weak broadband activity appeared at Halley from 0100 to 0300 UT and from 0630 to 0730 UT, in both cases in association with weak signals of riometer absorption. Intense Pc1–Pc2 activity began near 1000 UT at ~2 Hz, and fell rapidly in frequency. A second, higher-frequency wave component, also decreasing in frequency, appeared near 1200 UT. Intense waves appeared intermittently from ~1230 to 1900 UT, with frequencies between 0.6 and 1.2 Hz. The relatively diffuse signal at ~1.3–1.4 Hz appearing weakly between 0400 and 0700 and much more strongly after 1300 UT is again wind-related.

[31] V_{sw} and P_{sw} were at moderate levels throughout most of this day; no significant changes in either were evident in ACE data on this day until 1940 UT, when a short-lived 50% rise in V_{sw} and P_{sw} occurred.

[32] Wave spectrograms from SP and MC show only very weak signals corresponding to the intense waves seen from 1200 to 1900 at Halley. This is consistent with the evidently poor horizontal transmission of Pc1–Pc2 wave activity during the early recovery days of the August storm (Figures 3 and 4). The strongest wave activity at South Pole was broadband, occurring near 0330 UT in association with increased riometer absorption of similar duration. Riometer absorption at McMurdo was again near background levels, but again on this day weak Pc1–Pc2 waves appeared near local noon at McMurdo.

4. Superposed Epoch Analysis

[33] In order to characterize the 2005 Halley data set, we used Fourier spectrograms like those shown in Figures 3 and 4 to visually identify the beginning and end times of all Pc1–Pc2 wave emissions in the 0–2.5 Hz frequency range at Halley with power $\geq 10^{-4}$ nT^2-Hz^3 (in the yellow and red color ranges), and their center frequencies, and recorded them as events in hourly bins. Emissions at two or more frequencies were counted as separate events. Broadband ULF activity above the same power threshold was recorded separately.

[34] Figures 6 and 7 show superposed epoch plots of the occurrence of Pc1–Pc2 waves and broadband ULF noise at Halley as a function of UT for each day in the storm sequence. Because storm onset could occur at any UT, the epochs are not ordered by hours after onset, but by days after onset day. In both Figures 6 and 7, vertical dotted lines denote local midnight (0244 UT) and local noon (1444 UT). The effects of both storm time history and local time patterns will be evident in the analysis below.

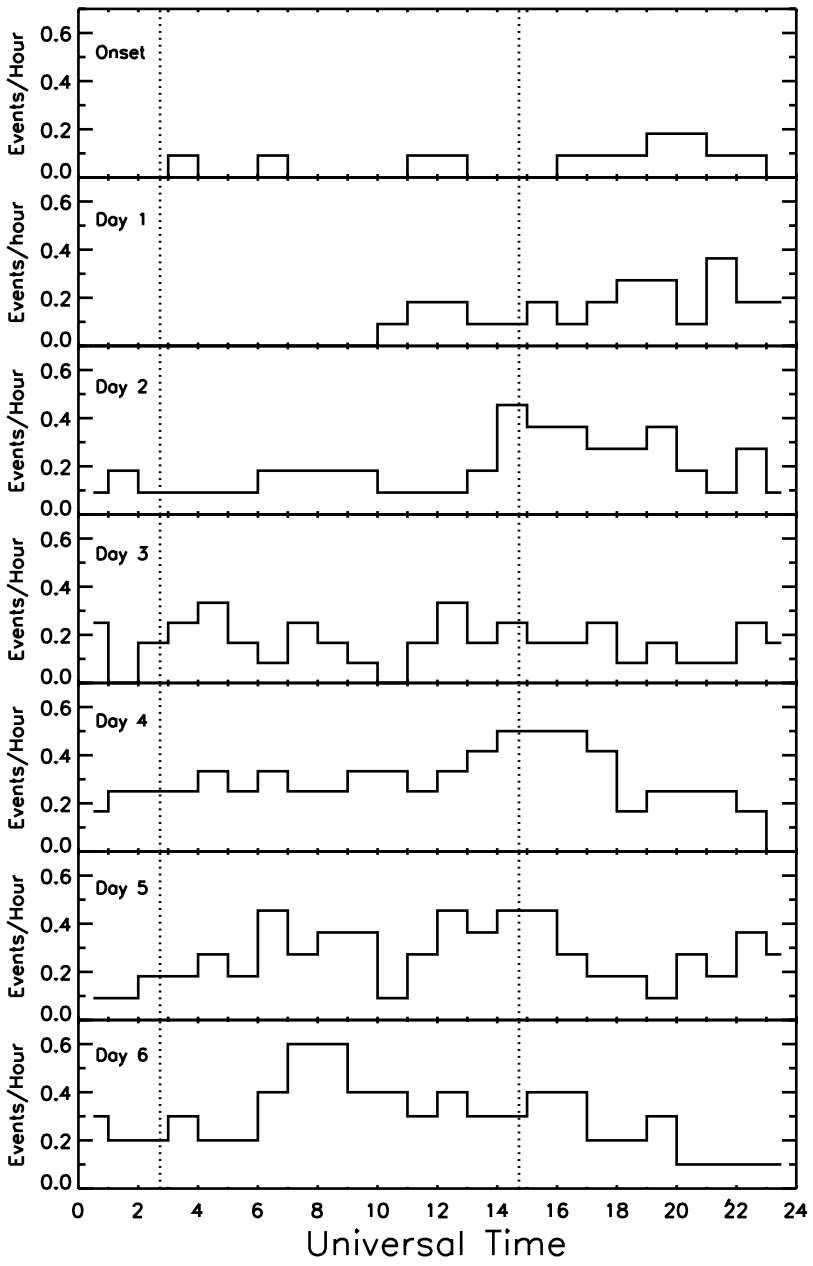

Figure 6. Superposed epoch plots of normalized hourly occurrence rate of strong to intense 0- to 1-Hz Pc1–Pc2 waves at Halley, as a function of universal time, shown for each day in the sequence of 13 storms. The times of local midnight (0244 UT) and local noon (1444 UT) are indicated by vertical dotted lines.

4.1. Occurrence of Pc1–Pc2 Waves

[35] Figure 6 shows that the local time distribution of 0–2.5 Hz Pc1–Pc2 wave events evolved from onset through recovery phase. The first panel shows Pc1–Pc2 events for the storm onset day. Because each storm onset occurred at a different UT, wave events in this panel include those both before and after onset. Waves occurred before storm onset on 20 May (0300–0400 UT), 24 August (0600–0700 UT), and 31 August (1100–1300 UT), all in association with modest increases in *Dst* that indicate compressions of the magnetosphere. Waves occurred later during the day of storm onset on 5 April, 12 April, 30 May, 23 June, and 18 July. With the exception of the 30 May storm, for which *Dst* reached −138, *Dst* for each of these latter storms did not extend below −100 nT, and most *Dst* minima occurred early in the day. It is notable, however, that no post-onset wave events were recorded before 1600 UT (∼13 magnetic local time, MLT).

[36] On the first day of the recovery phase, no narrow-band wave activity was observed on the ground for any of these storms before 1000 UT (∼07 MLT). Activity thereafter was steady, or exhibited a slight increase, toward dusk (2400 UT corresponds to ∼21 MLT). On day 2 there were a few events during local nighttime, but a clear diurnal peak was evident between 1400 and 2000 UT (∼11–17 MLT), the noon to dusk local time interval roughly consistent with

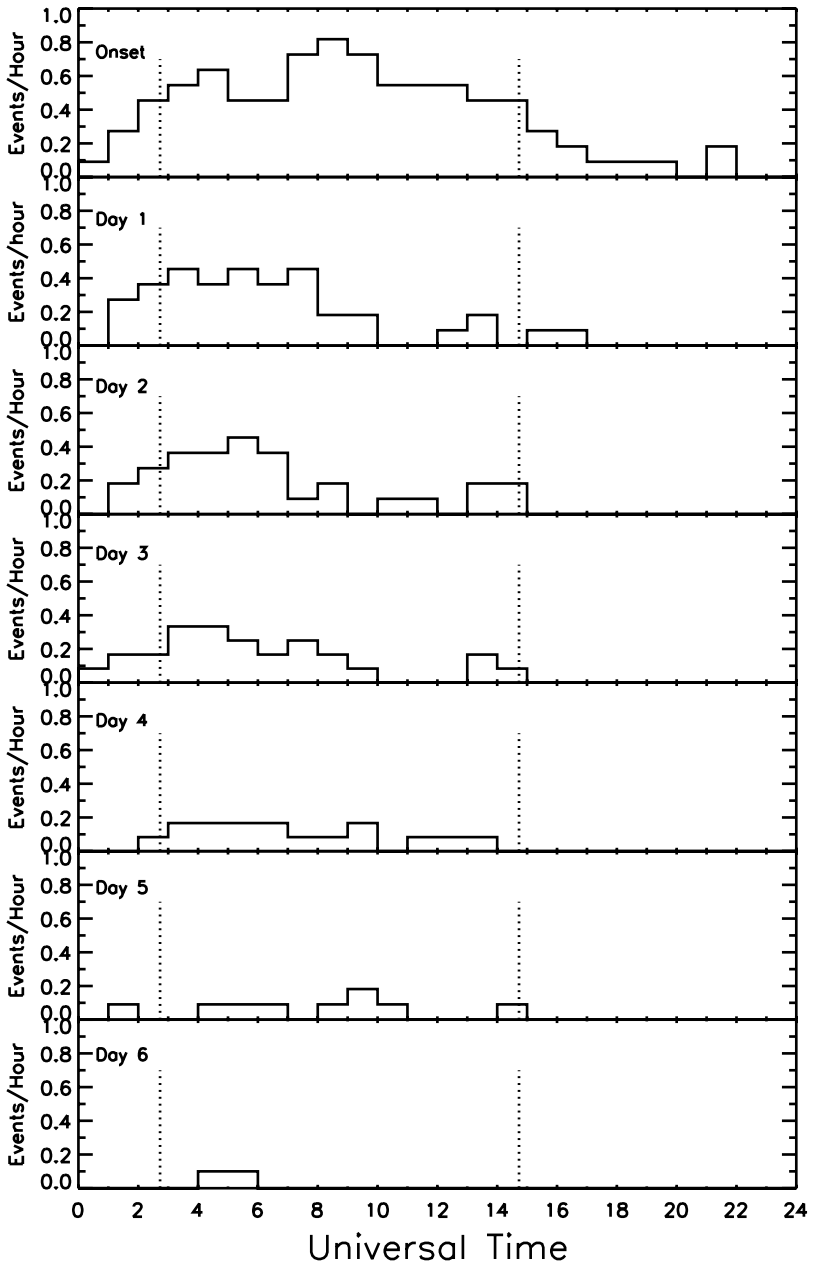

Figure 7. Superposed epoch plots of normalized hourly occurrence rate of strong to intense broadband ULF noise waves at Halley, as a function of universal time, shown for each day in the sequence of 13 storms.

the location of plasmaspheric plumes [*Moldwin et al.*, 2004]. As will be discussed below, the inferred "plume" appears in this data set as a noon-postnoon occurrence maximum, not a duskside maximum. Propagation effects, discussed below, would be more likely to attenuate or mask dayside wave power than duskside/nightside power, so this local time pattern is probably not simply an artifact of ground-based observations. The diurnal occurrence patterns for days 3 through 6 appear to be roughly even throughout all local times, although there is a trend from day 4 through day 6 for the times of peak occurrence to shift from local noon/early afternoon toward local morning.

[37] Comparison of individual storms within the set indicated a general tendency for Pc1 wave activity to begin a day earlier after weaker storms (at the end of the onset day or on day 1) than after stronger storms (on days 1 or 2), and the number and intensity of Pc1 wave events was generally stronger during the recovery periods of stronger storms.

4.2. Occurrence of Broadband Noise

[38] Occurrences of broadband ULF noise (characterized by strong or intense levels of wave power that increased to the lowest frequencies shown on the spectrograms, as in Figure 3) were also recorded for each day; occurrence rates are shown in Figure 7. Strong, often intermittent ULF noise was observed during the onset day of every storm, with duration ranging from 6 to nearly 22 h. ULF noise often became intense well before *Dst* reached its minimum value,

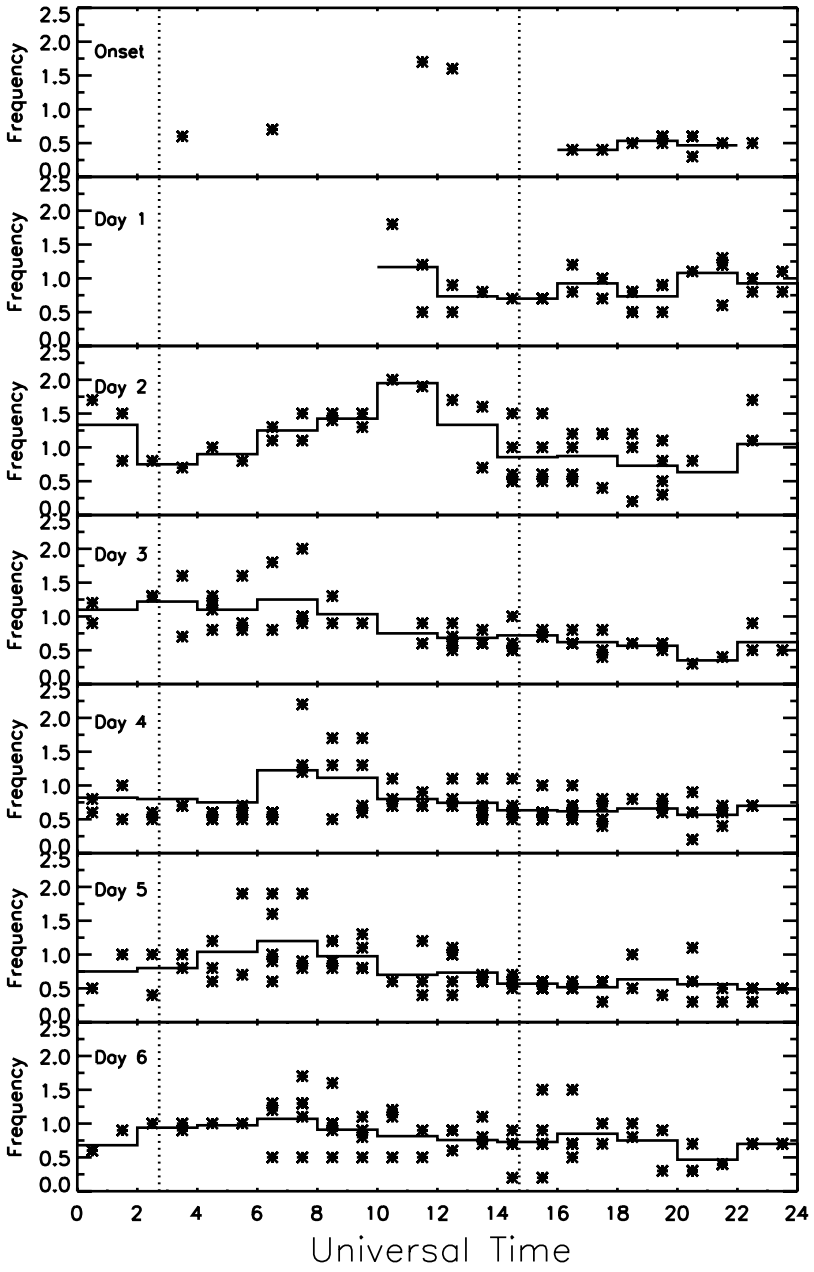

Figure 8. Superposed epoch plots of the frequency of Pc1–Pc2 waves observed at Halley, as a function of universal time, shown for each day in the sequence of 13 storms. The mean frequency for each 2-h interval is also indicated.

and continued a variable number of hours after this minimum. No narrowband activity was observed during any of these intervals. As Figure 7 indicates, broadband noise occurred most often during local nighttime and early morning hours at Halley (0000–0600 UT corresponds roughly to 21–03 MLT), but could occur at all local times in association with storm main phase. ULF noise also occurred with decreasing probability during successive days in the recovery phase of most but not all storms, but during these days was increasingly restricted to postmidnight to prenoon local times.

[39] The clear correlation between such ULF noise and riometer absorption in all events indicates strong precipitation of at least moderately energetic electrons (>5 keV) at these times – in most cases probably related to substorm injections.

4.3. Wave Frequency Distributions

[40] The frequencies of all Pc1–Pc2 wave events observed at Halley during this same 13-storm interval are shown in Figure 8, again as a function of storm day and UT. Each symbol denotes an hourly average of the center frequency of a strong wave Pc1–Pc2 wave event. (During a small number of days during the study interval two frequencies were recorded for specific hours, e.g., 0600–0700 UT on 27 August). The horizontal lines in each panel show the mean frequency for each 2-h interval.

Table 3. Mean Frequencies and Standard Deviations in Hz of Strong Pc1–Pc2 Waves Observed During the 13 Magnetic Storm Intervals in This Study, Listed as a Function of Storm Day, in Two UT/MLT Ranges[a]

	Frequency, Hz	
Day of Storm	0300–1200 UT (0–9 MLT)	1500–2400 UT (12–21 MLT)
0		0.48 ± 0.10
1	1.17 ± 0.65	0.89 ± 0.24
2	1.32 ± 0.38	0.84 ± 0.39
3	1.11 ± 0.37	0.59 ± 0.16
4	0.92 ± 0.42	0.61 ± 0.19
5	1.01 ± 0.41	0.53 ± 0.18
6	0.94 ± 0.32	0.75 ± 0.35

[a]Waves that occurred before storm onset are not included.

[41] The frequency of the Pc1–Pc2 wave events occurring after 1600 UT on the day of storm onset was near 0.5 Hz. As noted above, for most of these events the *Dst* index did not drop below −100 nT. On day 1 of the recovery phase, no waves were recorded before 1000 UT, and the wave frequency of most events was well above 0.5 Hz. The average wave frequency was higher on day 2 at almost all local times than on either prior or subsequent days. The highest-frequency waves appeared between 0600 and 1500 UT (in the prenoon local time sector, 3–12 MLT), but a population of lower-frequency waves, again near 0.5 Hz, was also evident from 1300 to 2000 UT (10–18 MLT). The frequency versus UT patterns observed during days 3–5 were quite similar: considerably higher frequencies were often observed between 0000 and 1000 UT (in the night-dawn sector, 21–07 MLT), than between 1000 and 2400 UT (07–21 MLT). The average frequency of dayside and postnoon waves declined sharply from day 2 to day 3, and then remained steady through day 5. The pattern for day 6 is less clear, as it contains both some of the lowest-frequency waves recorded during the study (<0.3 Hz, between 1400 and 2200 UT) and two postnoon events near 1.5 Hz.

[42] The trends evident in Figure 8 are summarized in Table 3, which lists the means and standard deviations of the frequencies of these events as daily averages over two UT/MLT ranges, corresponding to the dawn sector and the noon/dusk sector. The first four wave events during the onset day occurred before storm onset, and are thus not included in Table 3. Once dawn-sector waves appeared at Halley (in late morning on day 1), their mean frequency exceeded 1 Hz, peaking at 1.32 Hz on day 2. The mean value gradually fell to near 1 Hz by day 6, but the day-to-day variation remained high, especially between 0600 and 1200 UT (3–9 MLT). The frequency of waves in the noon-to-dusk sector was quite low (0.48 Hz) and narrowly distributed late on the day of onset, but was considerably higher (with a mean above 0.8 Hz but with large variation) on days 1 and 2. Mean frequencies on days 3–5 were near 0.6 Hz, with little variation. It is not clear whether the increased mean and standard deviation evident on day 6 are related to storm dynamics or other factors.

4.4. Inferences From the Ground-Based Data Set

[43] The above superposed epoch analysis and case studies demonstrate that very few Pc1–Pc2 events were observed during storm main phase and early recovery phase (1–2 days). Broadband noise was more common during onset. When waves did appear at Halley, their propagation to South Pole was suppressed. Increased occurrence of strong or intense waves began 1–4 days after onset, with a qualitative proportionality between storm intensity (parameterized by *Dst*) and length of delay. Waves could better propagate to higher latitudes during nighttime and during later stages of the recovery phase.

[44] With the exception of the interval 0800–0840 UT on 19 July all of the Pc1 wave events observed at South Pole were also observed, with equal or usually greater amplitude, at Halley. This allows us to infer that essentially all of the Pc1–Pc2 wave activity occurring in the outer magnetosphere in the Halley–South Pole local time sector during storm recovery phases was observed at Halley. We note, however, that Pc1–Pc2 activity can occur at *L* shells throughout the outer magnetosphere and extending nearly to the magnetopause, in particular during and after magnetospheric compressions or sudden impulses [*Olson and Lee*, 1983; *Kangas et al.*, 1986; *Anderson and Hamilton*, 1993; *Arnoldy et al.*, 2005] as well as after intervals of prolonged very quiet geomagnetic conditions [*Engebretson et al.*, 2002].

[45] Wave amplitudes observed at Halley can be used to infer amplitudes in space, using previously published simultaneous observations using other Antarctic search coil magnetometers and simultaneous observations from the AMPTE CCE [*Anderson et al.*, 1996] and Polar [*Engebretson et al.*, 2002; *Arnoldy et al.*, 2005] satellites. Although there were large variations in the ratio of satellite to ground amplitude (10, with uncertainties of +100% and −60%), the range of ratios was similar in each study. This variation may be caused by several factors: (1) variations in the spatial extent of the wave source regions, (2) wave absorption and/or partial reflection by heavy ions [*Rauch and Roux*, 1982; *Horne and Thorne*, 1993, 1994], which occur in the magnetosphere with variable concentrations, and (3) horizontal ducting of wave signals in the ionosphere over unknown distances from the flux tube on which the waves originated. *Fraser and Nguyen* [2001] also point out that in the presence of spatial variations in density in the E-region of the ionosphere, signals may not fall off monotonically with distance. The result is that for 1 Hz waves, a peak-to-peak amplitude of 1.5 nT in space corresponds to a spectral power of 10^{-4} nT^2-Hz^3 (yellow) at Halley, and a peak to peak amplitude of 5 nT in space corresponds to a spectral power of 10^{-3} nT^2-Hz^3 (red) at Halley. Waves in the Halley spectrograms with similar spectral power at different frequencies have amplitude that scales as 1/f.

5. POES Observations

[46] Precipitating 30-keV to 6.90-MeV proton fluxes measured by the MEPED detector on four POES satellites, each in low-altitude Sun-stationary orbit, were examined for evidence of precipitating ring current protons that could be associated with the waves observed at Halley.

[47] Figure 9 shows ULF spectrograms from Halley for 24–27 August and simultaneous *L* shell versus UT plots of precipitating and trapped 30- to 80-keV protons observed by the POES satellites. Plots of 80- to 250-keV protons

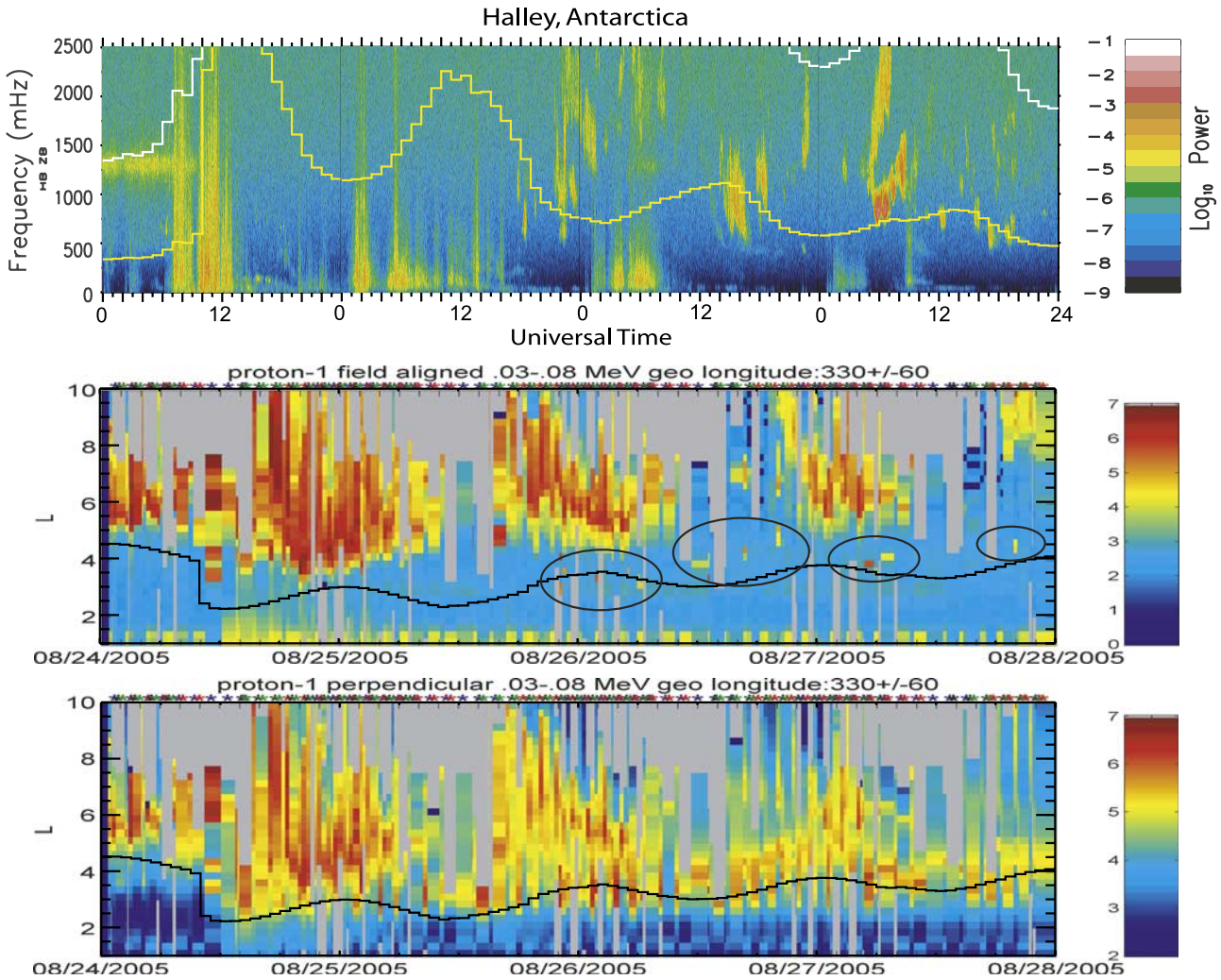

Figure 9. ULF spectrograms from Halley for 24–27 August 2005 and simultaneous *L* shell versus UT plots of precipitating and trapped 30- to 80-keV protons observed by the POES 15, 16, 17, and 18 satellites. The white and yellow traces superposed on the Halley spectrograms represent equatorial He^+ and O^+ gyrofrequencies, respectively, at the inferred plasmapause location, based on the *O'Brien and Moldwin* [2003] plasmapause model, and using the *Tsyganenko* [1996] model field. In each POES panel, precipitating fluxes are shown only for satellite passes within 60° geographic longitude of Halley (≤4 h local time east or west of Halley). Flux levels are designated according to the color bars at right. The black traces superposed on the POES proton spectrograms show the inferred hourly plasmapause location, also based on the model of *O'Brien and Moldwin* [2003] and the provisional *Dst* index. The ellipses in the second panel highlight the intervals of enhanced proton precipitation.

showed very similar patterns in nearly all details. In each POES panel, precipitating fluxes are shown only for satellite passes within 60° geographic longitude of Halley (≤4 h local time east or west of Halley). Flux levels are designated according to the color bars at right.

[48] Coincident with the sharp drop in *Dst* at storm onset, elevated proton fluxes, both precipitating and trapped, moved to lower *L* shells beginning near 1000 UT on 24 August. Trapped fluxes reached $L \sim 3$ by 1300 UT; their lower limit in *L* remained near that value throughout most of the following days, while precipitating fluxes (and hence the energetic proton isotropy boundary, as reviewed by *Yahnina et al.* [2003]) retreated toward higher *L* shells. Proton precipitation at all *L* shells declined to near background levels between local dawn (∼0900 UT) and noon (∼1500 UT) during each of the following days. Precipitation in the afternoon and night side continued to be intense at large *L* on each of the subsequent days, but retreated in *L* from ≥4 early on 25 August to ≥6 early on 27 August.

[49] The black traces superposed on both POES proton spectrogram panels show the inferred hourly plasmapause location, based on the model of *O'Brien and Moldwin* [2003] and using the provisional *Dst* index. It is evident that the location of the inner edge of the ring current matches well with the modeled plasmapause location. IMAGE RPI data also showed a low *L* value of the plasmapause ($L = 2.2$) at 1350 UT 24 August, consistent with both the POES observations and model results, but at

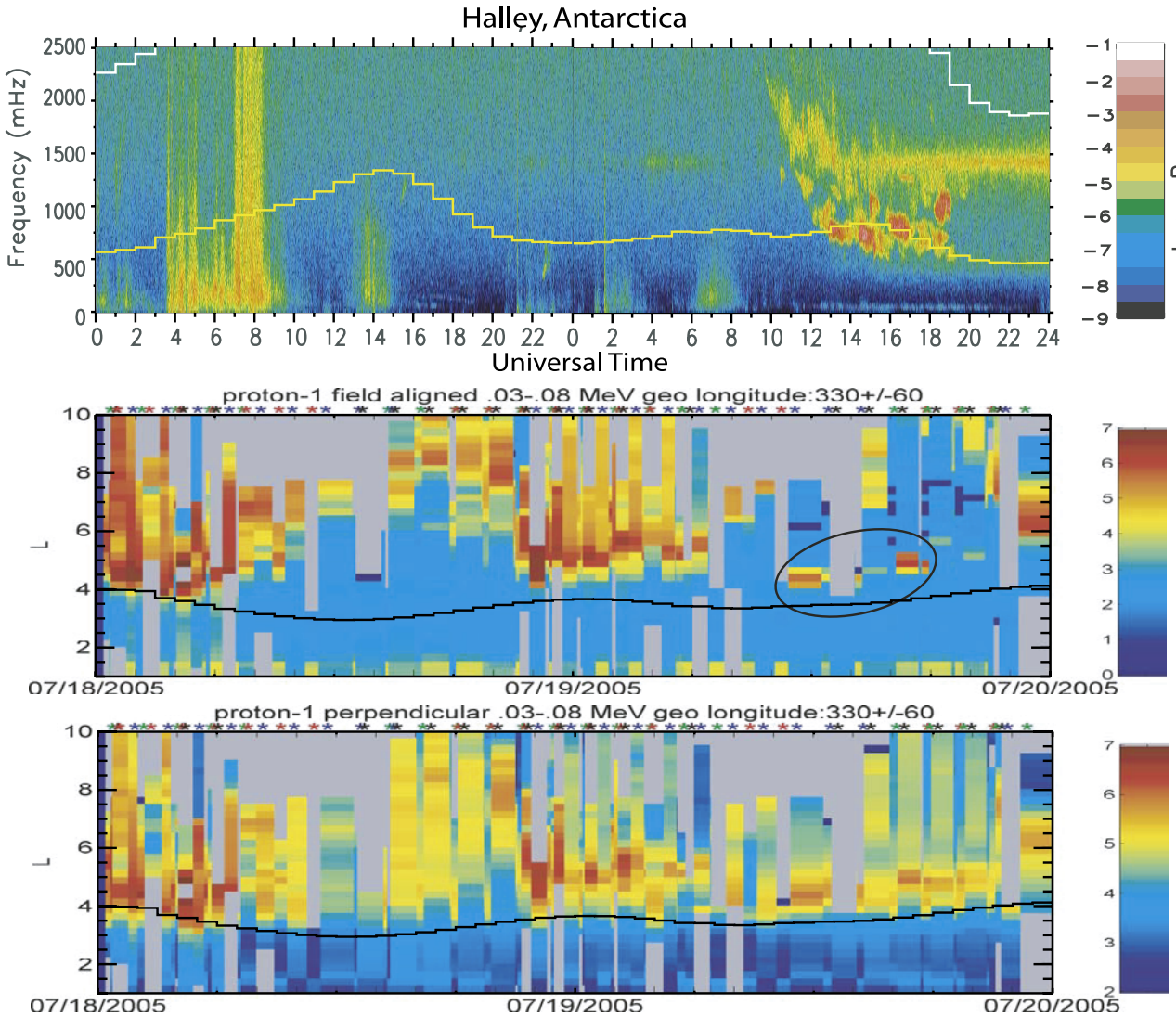

Figure 10. ULF spectrograms from Halley for 18–19 July 2005 and simultaneous L shell versus UT plots of precipitating and trapped 30- to 80-keV protons observed by the POES satellites, within 60° geographic longitude of Halley, as in Figure 9.

3.0 MLT, nearly 8 h earlier in local time than Halley [*Chi et al.*, 2006].

[50] Several localized intensifications of precipitating protons (yellow to red, each highlighted by an ellipse) can be seen in Figure 9, each of which occurred in rough coincidence with Pc1–Pc2 wave activity seen in the first panel. Localized intensifications of precipitating proton flux appeared near $L \sim 3$–4 late on 25 August and early on 26 August. Two similar intensifications of precipitation appeared near $L \sim 3$ after 1400 UT on 26 August. Intensifications of precipitation near $L = 4$ also appeared in the night side between 0500 and 0700 UT on 27 August. Finally, localized proton precipitation appeared near $L = 4.5$ near 1930 UT 27 August. Although not every wave event could be associated with intensifications of precipitating protons, this may well be an effect of the intermittent temporal and local time coverage of the four POES satellites.

[51] During each of these wave events precipitating protons were located at L shells near or up to 1 R_E outside the modeled plasmapause, but well equatorward of the energetic proton isotropy boundary. We note also that no localized intensifications of proton precipitation were observed earthward of these more extended high-latitude precipitation structures (within ±4 h local time of Halley) until the end of 25 August, when the first Pc1–Pc2 wave activity was observed.

[52] A similar comparison of POES and Halley data for 18–19 July is presented in Figure 10. The POES data in the second and third panels show that the inner edge of the ring current extended down to $L \sim 4$ or below from 0000 to 1000 UT on 18 July. Precipitating protons retreated to higher L shells after this time, however, and stayed above $L \sim 7$ until 2100 UT, when both trapped and precipitating fluxes again increased greatly and moved down to $L \sim 4$.

[53] Fluxes of trapped protons continued to peak between $L = 4$ and 5 during 19 July, but the isotropy boundary

retreated to large L after 0700 UT. The intense Pc1 wave activity observed at Halley beginning near 1000 UT on 19 July is reflected in the intense orange and red pixels in both the trapped and precipitating 30- to 80-keV protons (corresponding to increases of precipitating flux by factors of over 100), beginning at 1030 at $L \sim 4.5$ and 1600 UT at $L \sim 5$, respectively. Similar flux increases were observed in the 80–250 keV channel. Once again, no localized intensifications were observed during the main or early recovery phases of this storm.

[54] Also superposed on the Halley spectrograms (Figures 9 and 10, first panel) are traces of the He^+ (white) and O^+ (yellow) gyrofrequencies at the inferred plasmapause location, also based on the *O'Brien and Moldwin* [2003] plasmapause model, and using the *Tsyganenko* [1996] model field. Similar calculations assuming a dipole magnetospheric field produced similar frequencies, but with 10–25% lower values during local afternoon hours. The low-L plasmapause location throughout this 4-d period, and especially after storm onset, caused the local gyrofrequencies at the plasmapause to have quite large values. Waves that were observed at Halley were between the plasmapause He^+ and O^+ gyrofrequencies, or even below the O^+ gyrofrequency, in several cases straddling it. CRRES satellite observations by *Fraser and Nguyen* [2001] showed that very few waves appeared to be generated below f_c O^+. The fact that many of the observed waves in Figures 9 and 10 had frequencies comparable to the f_c O^+ value at the inferred plasmapause location suggests that these waves were not generated there, but in plasma trough regions with weaker magnetic fields.

6. Discussion

6.1. Comparison to Earlier Ground-Based Observations

[55] The occurrence patterns of ULF wave activity reported in our superposed epoch study compare well with those in early reports. The analysis of a 3-year data set from two sites in California by *Wentworth* [1964] showed that event occurrence was clearly maximized, by a factor of 2.5, during weeks following magnetic storms. Similarly, *Heacock and Kivinen* [1972] found that the temporal cross-correlations between *Dst* and Pc1 occurrence were largest with a delay of from 2 to 6 d, that is, wave occurrence maximized during poststorm periods. *Campbell* [1967] suggested that the relative absence of wave events in ground-based observations early in the magnetic storm sequence was due to ionospheric attenuation, which varied with the K_p index. Others have suggested wave absorption or reflection in the off-equatorial magnetosphere because of the presence of greatly increased fluxes of He^+ and O^+ (e.g., as reviewed by *Johnson and Cheng* [1999]). Both the early morning peak in wave frequency during the recovery phase, shown in Figure 8, and the shift toward a diurnal occurrence maximum during the later recovery phase, shown in the seventh panel of Figure 6, are consistent with early statistical summaries of observations by *Campbell and Stiltner* [1965] and *Fraser* [1968], made without regard to storm phase.

[56] A two-station superposed epoch study of structured and unstructured Pc1 pulsations at two Finnish stations (at $L = 3.3$ and 5.1) during 18 storms occurring during years of low solar activity [*Kerttula et al.*, 2001a, 2001b] showed considerably different temporal and diurnal patterns for these two categories of wave activity. In particular, their Figure 4a of temporal and diurnal occurrence patterns of structured wave activity is very similar to our Figure 6. As did earlier studies, *Kerttula et al.* [2001a] found that structured pulsations nearly vanished in ground records during storm main phase; occurrence increased to day 4 by a factor of about 4–5, with diurnal distributions changing from an afternoon-dusk sector peak on days 1–2 to a morning sector peak on later days. Unstructured Pc1 activity, however, occurred much less frequently at both stations, occurred mostly near local noon, and was only weakly affected by storm processes. *Kerttula et al.* [2001b] also noted a greater depletion of structured Pc1 events during more intense storms, again consistent with the qualitative result reported here.

[57] *Wentworth* [1964] also found that the character of signals in the 0.5–5 Hz frequency band was essentially the same during poststorm periods and quiet periods, but was statistically different from the activity observed during "storm days." In particular, during storm days roughly 80% of the observed activity was broadband and nonstructured, and another 6% was bursty noise or irregularly structured emissions, while during poststorm and quiet periods less than 20% was broadband and nonstructured, and no events appeared in the bursty noise or irregularly structured emission category. Our combined magnetometer and riometer observations suggest that these differences point not simply to different kinds of wave emissions, but to the presence on storm days (and at times during the succeeding days) of irregular signals generated at ionospheric altitudes as a result of substantially increased precipitation of energetic particles into the ionosphere.

[58] The Antarctic search coil and riometer observations reported here were also compared to those observed in the European sector by the Finnish search coil and wide-angle riometer chains, at a local time ~5 h MLT eastward. Broadband and narrowband wave activity observed from $L = 4.5$ to 5.9 were very similar to those at Halley during both storm intervals, as were observations of riometer absorption from $L = 3.8$ to 5.9 (not shown). In the data sets from both regions, broadband ULF activity was clearly associated with increased riometer absorption. As will be noted below, however, search coil observations at the lowest-latitude Finnish station ($L = 3.3$) showed some highly localized narrowband wave activity.

[59] Consistent with the lack of narrowband wave events during storm main phase in this study and in earlier ones, *Smith et al.* [2004] noted that compared with prestorm levels, VLF chorus intensity observed on the ground also decreased during storm main phase but was enhanced during the recovery phase. They attributed the main phase decrease to the disruption by storm-time electric fields of the well-defined ducts needed to guide whistler mode waves from their near-equatorial source region to the ionosphere. We note that ducting at the plasmapause density gradient was often also suggested in early studies of Pc1 pulsations to be important in guiding EMIC waves to the ground (e.g., as reviewed by *Rauch and Roux* [1982]).

6.2. Space-Based Observations

[60] Satellite observations of EMIC waves became available only later, during the decade of the 1970s, and are still relatively sparse during the onset of magnetic storms. *Bossen et al.* [1976] found, using magnetic field data from the geosynchronous ATS-1 satellite, that most of the Pc1 waves they observed occurred in the afternoon sector near dusk, and that Pc1 waves had a greatly increased occurrence rate within an 8-h interval centered on the main phase minimum of a magnetic storm with a −40 nT or lower *Dst* minimum. Substorm onsets are often associated with magnetic storms; *Bossen et al.* [1976] also found that almost every Pc1 event observed at ATS-1 was closely associated with a substorm expansion, with most events occurring within 1 h after an expansion onset. Simultaneous ground records showed the occurrence of IPDP events, another substorm-related wave signature, in most of the few available cases.

[61] *Bräysy et al.* [1998] used Freja electric field data from the Freja satellite (with apogee and perigee heights of 1750 and 600 km, respectively) to investigate the occurrence of ion cyclotron waves during the magnetic storm of April 1993. During the main phase, amplitudes were enhanced and the active wave region moved to considerably lower latitudes, and in the late evening local time sector (most events occurred from 18 to 24 MLT, but with other occurrences near 06 MLT). Their Figure 3 shows that only by day 3 of the storm did the MLT distribution return to being centered around noon, as it had been prior to storm onset. Finally, they noted that ground observations from three Finnish search-coil magnetometers showed weak Pc1 activity before the storm, a long interval of Pi (broadband) activity from storm onset through the following day, and no significant Pc1 activity at any of the three stations until late in the recovery phase.

[62] *Erlandson and Ukhorskiy* [2001] found, using Dynamics Explorer 1 data in the L range from 3.5 to 5.5, that the normalized EMIC wave occurrence rate was more than 5 times higher during storm time intervals (including both main phase and recovery phase) than during quiet intervals. Waves were also more common, and of higher intensity, in the dusk sector. They noted, however, that storm-related enhancements in magnetic fluctuations might mask storm events, so the ratio might be intrinsically even higher. In addition, they showed signatures of protons in the loss cone related to such waves, as expected from ion cyclotron instability theory.

[63] *Engebretson et al.* [2007] showed intense broadband noise in the transverse magnetic field components, as well as wave activity below the O^+ gyrofrequency in the field-aligned component, in a broad region across the geomagnetic equator ($4.5 < L < \sim 7$, MLT $\sim$ 9, $|\mathrm{MLAT}| < 25°$) in Cluster data during the early part of the main phase of the great October 2003 (Halloween) storm. Antarctic ground observations at $L > 6$ showed only intense broadband noise, similar to the observations reported here. It is notable, too, that all of the storm-time waves reported by *Bräysy et al.* [1998] were inferred to be below the equatorial He^+ gyrofrequency, and roughly half of them were below the O^+ gyrofrequency.

[64] Although it may be that the broadband noise associated with riometer absorption (overhead energetic particle precipitation) may have obscured any Pc1–Pc2 signals reaching Halley's location, it is also possible that propagation of such signals is impeded either at midlatitudes in the magnetosphere (by, e.g., heavy ion effects or absence of ducting), or in the ionosphere, during main phase intervals. The observations of *Bräysy et al.* [1998] of Pc1–Pc2 signals below 1750 km altitude certainly suggest the latter possibility.

6.3. Observations of Precipitating Protons

[65] As noted above, early theoretical studies of EMIC waves indicated that they would be effective in scattering ring current protons into the loss cone, and hence to precipitate into the ionosphere, and this was confirmed by *Erlandson and Ukhorskiy* [2001]. Localized precipitation of energetic protons was also noted in several cases by *Søraas et al.* [1980] using evening sector data from the ESRO-1 satellite, and was associated with IPDP events observed on the ground. A later study by *Søraas et al.* [1999] found localized enhancements of precipitating protons in the evening sector during the main phase of geomagnetic storms, and also noted a frequent association with the precipitation of energetic electrons as well. They noted in contrast that the localized enhancements in precipitation that were observed during the recovery phase tended to occur in the dayside, and did not include energetic electrons.

[66] *Yahnina et al.* [2003], in a study of one year's MEPED data from the NOAA 12 satellite, in a dawn-dusk orbit, found that isolated precipitating proton signatures equatorward of the isotropy boundary could be correlated in over 90% of the cases with ground-observed Pc1–Pc2 and/or IPDP waves when the satellite was within 2 h MLT of the Sodankylä Geophysical Observatory (L = 5.2). Similar correlations were observed in this study: of the 15 coincident POES-Halley events evident in Figures 9 and 10, 12 were observed when a POES spacecraft was within 2 h MLT of Halley (including all events on 19 July), and the other three within 4 h.

[67] *Yahnina et al.* [2003] found that their type 2 events, proton precipitation associated with IPDP, had a maximum occurrence in the evening sector, and were observed mainly during large negative *Dst*, which is associated with the main or early recovery phase of geomagnetic storms. Our observations indicate that proton precipitation can occur at various local times: during the night sector as well as day and evening. All the associated wave and proton precipitation events we observed occurred during the recovery phase, in regions of strong ring current, and were situated on L shells between the isotropy boundary and the plasmapause. We note that the location of these precipitation events in L, between the plasmapause and the auroral zone, is consistent with the location of subauroral proton precipitation events observed by the Spectrographic Imager onboard the NASA-IMAGE satellite [*Immel et al.*, 2005]. In that study, Pc1 pulsations were also observed on the ground in the vicinity of each of the subauroral proton arcs studied.

[68] Finally, we stress that there was no evidence of localized precipitation during the main and early recovery phases of the July and August 2005 storms. To the extent that one can assume a connection between EMIC wave generation and such precipitation, consistent with the studies cited above, this suggests that in fact no EMIC waves

were generated equatorward of the isotropy boundary during these times.

6.4. Poleward Propagation of Wave Activity

[69] The horizontal attenuation of Pc1–Pc2 waves has also been studied since early in the space age. *Tepley and Landshoff* [1966] and *Manchester* [1966] presented the first waveguide theory for ionospheric propagation of hydromagnetic emissions (near the Alfven or phase velocity minimum near the F2 peak), and suggested that daytime waves would be significantly attenuated. *Manchester and Fraser* [1970] studied the horizontal propagation of Pc1 signals in the ionospheric duct: Maximum signal attenuation in the duct occurred in midday-afternoon hours when the E region electron density was maximum, and minimum attenuation occurred near 0500 LT. *Heacock and Kivinen* [1972] noted the attenuation of Pc1–Pc2 signals toward higher latitudes, and suggested that ionospheric disturbances (such as spread F) associated with storm and/or substorm activity would rather effectively scatter and attenuate Pc1 waves propagating poleward in the ionospheric duct. *Heacock and Akasofu* [1973] noted that the amplitudes of Pc1 events at sites very near the geomagnetic poles, Thule and Vostok, were almost always quite small, and attributed any amplitude variations to variations in propagation conditions in the F layer waveguide rather than variations in the distance to the source region.

[70] This study has demonstrated that although the same waves observed at Halley were often observed at South Pole and McMurdo, they were greatly attenuated during the early part of the recovery phase, and were more severely attenuated during daytime than during nighttime hours. We note, too, that the broadband ULF noise observed during and after main phase was consistently local, that is, consistent with locally observed riometer absorption, but ULF noise and riometer absorption observed at Halley and at South Pole were largely independent of each other. Both results are of interest in providing constraints on the interpretation of the absence of Pc1–Pc2 waves in ground data during and shortly after storm main phase.

[71] It is significant to note that between 1400 and 1500 UT on 25 August, strong 1.5 Hz pulsation activity was observed at the lowest-latitude Finnish station, Nurmijarvi (L = 3.3), possibly stimulated by the increase in solar wind pressure at that time (Figure 3), but was not seen at L = 4.5 or higher. Similarly, and consistent with the diurnal pattern in propagation observed in this and earlier studies, strong 2 Hz activity was observed at L = 3.3 at 2300 UT, only a weak 2 Hz signal was observed at L = 4.5, and no signal was observed at the higher-latitude stations. This observation of EMIC waves at lower L on the first day of storm recovery, and their absence at even moderately higher L values, suggests the possibility that EMIC waves generated nearer to or even inside the plasmapause might not propagate to Halley during the early stages of magnetic storms. Our observations thus support the earlier conclusion of *Kerttula et al.* [2001a, 2001b], who studied storm-time Pc1 activity using two of the stations in the Finnish chain at L = 3.3 and 5.1, that on days 1 and 2 stations can only register waves having their foot point near that station.

6.5. *L* shell and Local Time Dependence

[72] It has been a common feature of theoretical models of EMIC wave growth during magnetic storm periods to show strong localization near the plasmapause, at least during the main and early recovery phases [*Jordanova et al.*, 1996, 2001; *Khazanov et al.*, 2006], because of the suppression of wave refraction at the plasmapause density gradient. Although our data set can say nothing about wave location during main phase, our observations that the waves observed during the recovery phase were generated outside the plasmapause is not consistent with this prediction. *Kerttula et al.* [2001a, 2001b] also interpreted their multistorm, two-station observations as not supporting a plasmapause source location during the recovery phase.

[73] As shown in Figures 9 and 10, satellite-based observations of the L shells of precipitating ring current protons and ground-based observations of wave frequency can be compared to the modeled location of the plasmapause and consequent calculations of the expected gyrofrequencies at these locations, respectively. Both comparisons suggest that most or all of the observed wave activity during the recovery phase was generated outside the plasmapause, either in the plasma trough or in dayside plume regions, again consistent with the observations of *Fraser and Nguyen* [2001].

[74] *Fraser and Nguyen* [2001] reviewed many early studies that suggested that regions near or just outside the plasmapause might be preferred locations for EMIC wave growth. Their studies of Pc1–Pc2 wave data throughout the lifetime of the CRRES satellite, however, showed that the plasmapause is not the preferred site for wave generation and propagation. Instead, and consistent with the earlier AMPTE CCE observations of *Anderson et al.* [1992a, 1992b], they found that the probability of wave occurrence increased with radial distance (L value). In particular, although events were observed over a range of L values both inside and outside the plasmapause, they found that most events occurred more than 1 R_E outside the plasmapause. Their observations did, however, suggest that afternoon sector waves were associated with the plasmapause bulge and possibly detached plasma regions. Detailed support for such an association has been provided by recent studies by *Fuselier et al.* [2004], who found that the limited latitudinal extent of proton auroral emissions (presumably related to Pc1–Pc2 wave generation) appeared to be related to the interaction between hot ring current protons and cold plasmaspheric ions, by *Spasojević et al.* [2004], who reported an example for which a long-duration subauroral proton arc was closely associated with a duskside plasmaspheric plume, and by *Fraser et al.* [2005], who observed EMIC waves in GOES satellite data within such plumes that extended to geosynchronous orbit.

[75] The local time distribution of Pc1–Pc2 wave events shown in Figure 6 can be compared to both the results of satellite-based observational studies and to theoretical expectations. AMPTE CCE data analyzed by *Anderson et al.* [1992a] showed roughly uniform occurrence in MLT for L below 5, but with a peak in the prenoon to midnight sector for L between 5 and 6. Beyond L = 7 the occurrence distribution was dominated by daytime (dawn to dusk) events, but with a modest postnoon peak. The CRRES data

showed an occurrence maximum during afternoon hours, but this was not broken down by L shell.

[76] *Anderson et al.* [1992b] presented normalized frequency distributions, indicating that waves in the prenoon to dusk sector (10–19 MLT) were usually observed in bands above and below f_cHe^+, while waves in the 03–10 MLT sector were characterized by $f/f_cH^+ \sim 0.5$. Their Figure 2 indicated higher frequencies near dawn than in the noon-afternoon sector for all L shells beyond 5, but a relatively flat distribution below $L = 5$. The MLT distribution of spectral power observed by AMPTE CCE was relatively flat below $L = 5$, but at higher L values exhibited a broad peak centered near dusk. Our observations of higher-frequency waves near dawn (Figure 8) are consistent with the *Anderson et al.* [1992b] results, although of course the L shells where the waves originated cannot be determined from ground-based observations alone.

[77] We note that neither the AMPTE CCE nor CRRES study attempted to parameterize their waves according to storm epoch, so their results can be compared only to an "average" of the patterns seen in Figures 6 and 8. However, simulations by *Jordanova et al.* [1996] suggested that magnetospheric particle distributions in the later recovery phase favor the generation of Pc1 pulsations in the morning MLT sector. The panels for days 3–6 in Figure 6 appear to be consistent with this prediction: occurrence actually maximizes in the dawn sector (0600–1200 MLT, or 0300–0900 UT) on day 6.

6.6. Implications for Radiation Belt Dynamics

[78] One of the key issues in understanding the radiation belts is determining what is responsible for the rapid drop in MeV electron flux during the storm main phase. Two principal mechanisms have been suggested. The first is that waves scatter the MeV electrons into the atmosphere; one of the most likely candidates for this is EMIC waves. The other idea is that the electrons become detrapped (i.e., are no longer on closed drift paths that encircle the Earth) and encounter the magnetopause and are lost. The relative contribution to each mechanism is unknown. One of the ways of testing the loss to the atmosphere is to identify whether EMIC waves are observed at the same time as the rapid flux dropouts during the main phase.

[79] A recent study by *Bortnik et al.* [2006], using data from a variety of satellites including POES and SAMPEX, suggested that both of these mechanisms were operative during the onset of the great magnetic storm of 20 November 2003: for $L > 5$, losses to the magnetopause dominated, but for $L < 5$, rapid losses were energy-dependent in ways consistent with interactions with whistler mode chorus waves, plasmaspheric hiss, and EMIC waves at different parts of the drift orbits of the energetic electrons.

[80] As noted above, on the basis of ground-based ULF observations, there is very little evidence for the occurrence of EMIC waves during the storm main phase. In this study as in all previous ground-based investigations, no such waves were observed. However, the consistent presence of intense broadband ULF wave power (Pi activity) and its associated strong riometer absorption during each of the storms studied suggest that intense, possibly turbulent wave power may exist in the middle magnetosphere and serve as an efficient mechanism for precipitating energetic particles. Indeed, the early study of *Heacock and Kivinen* [1972] suggested that the ion cyclotron turbulence studied theoretically by *Cornwall et al.* [1970] was not necessarily to be identified with narrowband Pc1 waves observed on the ground, though the cyclotron instability would be the operative wave-particle energy transfer mechanism in both cases. They suggested that the turbulence might be a nonpropagating form of disturbance that would not be detected on the ground. Our recent observations of purely compressional oxygen-band waves during the main phase of the great October 2003 (Halloween) storm, which were accompanied by intense broadband activity in the transverse components [*Engebretson et al.*, 2007], also gives in situ support for the importance of turbulent processes that have not heretofore been considered.

[81] Assuming that such waves are generated in the middle and/or inner magnetosphere near the equator, by what means might they be prevented from reaching the ground? One mechanism suggested in early studies, reflection of waves at midlatitudes where the wave frequency matches the local bi-ion frequency, requires substantial concentrations of heavy ions, which are expected and observed during large magnetic storms, but not during more moderate ones. On the other hand, intense precipitation of electrons might enhance ionospheric absorption of the waves. *Kerttula et al.* [2001a, 2001b], for example, argued that deterioration of both the ionospheric Alfven resonator and ionospheric ducting during the storm main phase might prevent waves from reaching the ground, although they did not specify any mechanism for this deterioration. Given the highly variable levels of O^+ and He^+ that have been observed during magnetic storms, the observation of broadband ULF noise during every one of the storms in this study suggests that this latter mechanism of wave screening (by enhanced electron precipitation) is at least plausible, and should be investigated further.

7. Summary and Conclusions

[82] This study of Pc1–Pc2 waves observed at Halley, Antarctica ($L = 4.5$) during and after magnetic storms has shown the following:

[83] 1. We have confirmed the observations of several earlier ground-based magnetometer studies that Pc1–Pc2 waves appear most often during the late recovery phase (3–6 days later), not during and shortly after onset. Occurrence and frequency characteristics of these waves also agree with those found earlier.

[84] 2. In addition, however, magnetometers see intense broadband noise during storm main phase, in close association with often-intense overhead precipitation of >5 keV electrons (as detected by riometers). These signatures, although implicit in the early observations of *Wentworth* [1964], have been neglected in most discussions of the occurrence and propagation of Pc1–Pc2 waves during storms.

[85] The contrast between the absence of Pc1–Pc2 waves in ground-based records during and immediately after storms, and their reported presence in space-based observations, has typically been explained by a presumed failure of Pc1–Pc2 waves to propagate from space to the ground. It is not yet clear whether EMIC waves are absent because of the

intense electron precipitation and the broadband ULF noise it generates can obscure EMIC wave signals in magnetometer records, whether these or other physical processes attenuate or reflect these waves before they can reach the ground, or even whether other wave modes (including turbulence) are dominant in space at such times. At least some storm-time Pc1–Pc2 waves, for example, are now known to be purely compressional [*Engebretson et al.*, 2007]. The example of 26 August 2005, however, shows that moderate levels of ULF noise (accompanied by moderate levels of riometer absorption) clearly do not obscure higher-frequency waves.

[86] 3. Our observations in the early recovery phase of magnetic storms are consistent with suggestions that many Pc1–Pc2 waves are generated in afternoon-sector plasmaspheric plumes. Waves are most commonly observed in the prenoon-to-dusk sector during the first two days of the recovery phase, but later become more equally distributed across local time. If, as is likely, such plumes are the source of these waves during the first days of the recovery phase, they occur earlier in the day than is often suggested in pictorial models: our data show a relative absence of wave events in the postdusk local time sector.

[87] 4. Analysis of POES proton data during two storm intervals has shown that trapped 30- to 250-keV protons (the bulk of the ring current) do indeed extend earthward to approximately the plasmapause, as modeled using the *O'Brien and Moldwin* [2003] local time–dependent model. In addition, both POES proton data and frequency comparisons suggest that nearly all of the waves observed during the recovery phase originate outside the plasmapause.

[88] 5. Our comparisons of Pc1–Pc2 waves at Halley and POES proton precipitation data during storm recovery phase also confirm earlier studies supporting a strong association between EMIC waves and the precipitation of ring current protons. The absence of precipitation signatures during the main and early recovery phase, however, is a new result. Rather than the absence of waves in ground records being the result of propagation effects, this suggests the possibility that EMIC waves simply did not occur during these times.

[89] 6. We have also found evidence confirming the observations of *Kerttula et al.* [2001a] that during the early storm recovery phase the poleward propagation of Pc1–Pc2 waves through the ionospheric waveguide is more severely attenuated. This suggests the possibility that EMIC waves generated at lower L shells, near or even inside the plasmapause, might not propagate to Halley during the early stages of magnetic storms. Although we have found no evidence of localized proton precipitation in POES data at lower L shells at Halley's longitude in the two case studies presented here, we have noted the presence of two wave events at L = 3.3 in Finland on 25 August 2005. In at least one of these events, the location also appears to be well outside the plasmapause.

[90] Although the available satellite studies using AMPTE CCE and CRRES also suggest that most wave events occurred outside the plasmapause, these studies did not consider storm phase, so further characterization of the occurrence of storm-time EMIC waves near the plasmapause must await future space-based studies, notably by the planned Radiation Belt Storm Probe spacecraft.

[91] If further study confirms that these waves originate outside the plasmapause, this would have important consequences for our understanding of the loss of radiation belt electrons. From a survey of a subset of CRRES data, *Meredith et al.* [2003] found that EMIC waves could resonate with electrons with energies down to 500 keV in high-density regions. Outside the plasmapause, however, the resonant electron energy will be higher owing to the lower density. It thus remains to be shown whether EMIC waves are a dominant loss process for radiation belt electrons at energies of ~1 MeV during magnetic storms.

[92] There are still very few satellite-based studies of EMIC waves or ULF turbulence during the main phase of magnetic storms. Although this study provides further evidence that no EMIC waves are seen on the ground during storm main phase, the physics behind this absence is still not clear. Other processes, perhaps related to strong transverse turbulence of the sort observed by Cluster during the 29 October 2003 storm [*Engebretson et al.*, 2007] may play a more prominent role in particle loss processes during the initial phase of magnetic storms than has previously been considered.

[93] **Acknowledgments.** We thank both referees for their critical and constructive comments, and we thank Paul O'Brien of the Aerospace Corporation for his support and helpful suggestions. Steven Quick, Allison Matts, Ashley Westerman, Nathan Otto, Michael Murphy, and Matt Broughton of Augsburg College assisted in processing the search coil data and compiling the occurrence database. Kent Bodurtha of Augsburg College provided the modeled plasmapause locations and predicted gyrofrequencies, and Haje Korth of JHU/APL supplied the Tsyganenko magnetic field model routines. Search coil observations at Halley, South Pole, and McMurdo are supported by National Science Foundation grants ANT-0442648 and ANT-0538379 to Augsburg College and by NSF grants ANT-0442787 and ANT-0538474 to the University of New Hampshire. Riometer observations at South Pole and McMurdo are supported by NSF grants OPP-0338105 and OPP-0341470 to Siena College.

[94] Zuyin Pu thanks Robert E. Erlandson and another reviewer for their assistance in evaluating this paper.

References

Albert, J. M. (2003), Evaluation of quasi-linear diffusion coefficients for EMIC waves in a multispecies plasma, *J. Geophys. Res.*, *108*(A6), 1249, doi:10.1029/2002JA009792.

Anderson, B. J., and D. C. Hamilton (1993), Electromagnetic ion cyclotron waves stimulated by modest magnetospheric compressions, *J. Geophys. Res.*, *98*, 11,369–11,382.

Anderson, B. J., R. E. Erlandson, and L. J. Zanetti (1992a), A statistical study of Pc 1–2 magnetic pulsations in the equatorial magnetosphere: 1. Equatorial occurrence distributions, *J. Geophys. Res.*, *97*, 3075–3088.

Anderson, B. J., R. E. Erlandson, and L. J. Zanetti (1992b), A statistical study of Pc 1–2 magnetic pulsations in the equatorial magnetosphere: 2. Wave properties, *J. Geophys. Res.*, *97*, 3089–3101.

Anderson, B. J., R. E. Erlandson, M. J. Engebretson, J. Alford, and R. L. Arnoldy (1996), Source region of 0.2 to 1.0 Hz geomagnetic pulsation bursts, *Geophys. Res. Lett.*, *23*, 769–772.

Arnoldy, R. L., et al. (2005), Pc1 waves and associated unstable distributions of magnetospheric protons observed during a solar wind pressure pulse, *J. Geophys. Res.*, *110*, A07229, doi:10.1029/2005JA011041.

Bortnik, J., R. M. Thorne, T. P. O'Brien, J. C. Green, R. J. Strangeway, Y. Y. Shprits, and D. N. Baker (2006), Observation of two distinct, rapid loss mechanisms during the 20 November 2003 radiation belt dropout event, *J. Geophys. Res.*, *111*, A12216, doi:10.1029/2006JA011802.

Bossen, M., R. L. McPherron, and C. T. Russell (1976), A statistical study of Pc1 magnetic pulsations at synchronous orbit, *J. Geophys. Res.*, *81*, 6083–6091.

Bräysy, T., K. Mursula, and G. Marklund (1998), Ion cyclotron waves during a great magnetic storm observed by Freja double-probe electric field instrument, *J. Geophys. Res.*, *103*, 4145–4155.

Campbell, W. H. (1967), Low attenuation of hydromagnetic waves in the ionosphere and implied characteristics in the magnetosphere for Pc1 events, *J. Geophys. Res.*, *72*, 3429–3445.

Campbell, W. H., and E. C. Stiltner (1965), Some characteristics of geomagnetic pulsations at frequencies near 1 c/s, *Radio Sci.*, *69*, 1117–1132.

Chi, P. J., C. T. Russell, M. Spasojevic, D. L. Carpenter, and J. Tu (2006), Storm-time plasmaspheric depletion and refilling as observed by joint mass and charge density measurements, *Eos Trans. AGU*, *87*(52), Fall Meet. Suppl., Abstract SM13B-04.

Chivers, H. J. A. (1975), High-latitude ionospheric absorption, *Antarct. J. U. S.*, *10*, 222.

Cornwall, J. M. (1965), Cyclotron instabilities and electromagnetic emission in the ultra low frequency and very low frequency ranges, *J. Geophys. Res.*, *70*, 61.

Cornwall, J. M., F. V. Coroniti, and R. M. Thorne (1970), Turbulent loss of ring-current protons, *J. Geophys. Res.*, *75*, 4699–4709.

Daglis, I. A., R. M. Thorne, W. Baumjohann, and S. Orsini (1999), The terrestrial ring current: Origin, formation, and decay, *Rev. Geophys.*, *37*, 407–438.

Dudeney, J. R., A. S. Rodger, A. J. Smith, M. J. Jarvis, and K. Morrison (1995), Satellite Experiments Simultaneous with Antarctic Measurements (SESAME), *Space Sci. Rev.*, *71*, 705–742.

Dudeney, J. R., R. B. Horne, M. J. Jarvis, R. I. Kressman, A. S. Rodger, and A. J. Smith (1997), British Antarctic Survey's ground-based activities complementary to satellite missions such as Cluster, in *Satellite–Ground Based Coordination Sourcebook*, edited by M. Lockwood, M. N. Wild, and H. J. Opgenoorth, *Eur. Space Agency Spec. Publ.*, *ESA SP-1198*, 101–110.

Engebretson, M. J., et al. (1997), The United States automatic geophysical observatory (AGO) program in Antarctica, in *the Satellite–Ground Based Coordination Sourcebook*, edited by M. Lockwood, M. N. Wild, and H. J. Opgenoorth, *Eur. Space Agency Spec. Publ.*, *ESA-SP-1198*, 65–99.

Engebretson, M. J., W. K. Peterson, J. L. Posch, M. R. Klatt, B. J. Anderson, C. T. Russell, H. J. Singer, R. L. Arnoldy, and H. Fukunishi (2002), Observations of two types of Pc 1–2 pulsations in the outer dayside magnetosphere, *J. Geophys. Res.*, *107*(A12), 1451, doi:10.1029/2001JA000198.

Engebretson, M. J., A. Keiling, K.-H. Fornacon, C. A. Cattell, J. R. Johnson, J. L. Posch, S. R. Quick, K.-H. Glassmeier, G. K. Parks, and H. Rème (2007), Cluster observations of Pc 1–2 waves and associated ion distributions during the October and November 2003 magnetic storms, *Planet. Space Sci.*, *55*, 829–848, doi:10.1016/j.pss.2006.03.015.

Erlandson, R. E., and A. J. Ukhorskiy (2001), Observations of electromagnetic ion cyclotron waves during geomagnetic storms: Wave occurrence and pitch angle scattering, *J. Geophys. Res.*, *106*, 3883–3895.

Evans, D. S., and M. S. Greer (2000), Polar-Orbiting Environmental Satellite Space Environment Monitor 2: Instrument description and archive data documentation, *NOAA Tech. Memo OAR SEC-93*, NOAA, Boulder, Colo. (Available at http://www.ngdc.noaa.gov/stp/NOAA/docs/SEM2v1.4b.pdf)

Fraser, B. J. (1968), Temporal variations in Pc1 geomagnetic micropulsations, *Planet. Space Sci.*, *16*, 111–124.

Fraser, B. J., and T. S. Nguyen (2001), Is the plasmapause a preferred source region of electromagnetic ion cyclotron waves in the magnetosphere?, *J. Atmos. Sol. Terr. Phys.*, *63*, 1225–1247.

Fraser, B. J., H. J. Singer, M. L. Adrian, D. L. Gallagher, and M. F. Thomsen (2005), The relationship between plasma density structure and EMIC waves at geosynchronous orbit, in *Inner Magnetosphere Interactions: New Perspectives From Imaging*, *Geophys. Monogr. Ser.*, vol. 159, edited by J. Burch, M. Schulz, and H. Spence, pp. 55–70, AGU, Washington, D. C.

Fujita, S. (1987), Duct propagation of a short-period hydromagnetic wave based on the International Reference Ionosphere model, *Planet. Space Sci.*, *35*, 91–103.

Fujita, S., and T. Tamao (1988a), Duct propagation of hydromagnetic waves in the upper ionosphere: 1. Electromagnetic field distributions in high latitudes associated with localized incidence of a shear Alfven wave, *J. Geophys. Res.*, *93*, 14,665–14,673.

Fujita, S., and T. Tamao (1988b), Duct propagation of hydromagnetic waves in the upper ionosphere: 2. Dispersion characteristics and loss mechanisms, *J. Geophys. Res.*, *93*, 14,674–14,682.

Fuselier, S. A., S. P. Gary, M. F. Thomsen, E. S. Claflin, B. Hubert, B. R. Sandel, and T. Immel (2004), Generation of transient dayside subauroral proton precipitation, *J. Geophys. Res.*, *109*, A12227, doi:10.1029/2004JA010393.

Greifinger, C., and P. S. Greifinger (1968), Theory of hydromagnetic propagation in the ionosphere wave guide, *J. Geophys. Res.*, *73*, 7473–7490.

Hayakawa, M., S. Shimakura, T. Kobayashi, and N. Sato (1992), A study of polarization of irregular pulsations of diminishing period and their generation mechanism, *Planet. Space Sci.*, *40*, 1081–1091.

Heacock, R. R., and S.-I. Akasofu (1973), Periodically structured Pc1 micropulsations during the recovery phase of intense magnetic storms, *J. Geophys. Res.*, *78*, 5524–5536.

Heacock, R. R., and M. Kivinen (1972), Relation of Pc1 micropulsations to the ring current and geomagnetic storms, *J. Geophys. Res.*, *77*, 6746–6760.

Horne, R. B., and R. M. Thorne (1993), On the preferred source location for the convective amplification of ion cyclotron waves, *J. Geophys. Res.*, *98*, 9233–9247.

Horne, R. B., and R. M. Thorne (1994), Convective instabilities of electromagnetic ion cyclotron waves in the outer magnetosphere, *J. Geophys. Res.*, *99*, 17,259–17,273.

Immel, T. J., S. B. Mende, H. U. Frey, J. Patel, J. W. Bonnell, M. J. Engebretson, and S. A. Fuselier (2005), ULF waves associated with enhanced subauroral proton precipitation, in *Inner Magnetosphere Interactions: New Perspectives From Imaging*, *Geophys. Monogr. Ser.*, vol. 159, edited by J. Burch, M. Schulz, and H. Spence, pp. 71–84, AGU, Washington, D. C.

Johnson, J. R., and C. Z. Cheng (1999), Can ion cyclotron waves propagate to the ground?, *Geophys. Res. Lett.*, *26*, 671–674.

Jordanova, V. K., L. M. Kistler, J. U. Kozyra, G. V. Khazanov, and A. F. Nagy (1996), Collisional losses of ring current ions, *J. Geophys. Res.*, *101*, 111–126.

Jordanova, V. K., C. J. Farrugia, R. M. Thorne, G. V. Khazanov, G. D. Reeves, and M. F. Thomsen (2001), Modeling ring current proton precipitation by EMIC waves during the May 14–16, 1997 storm, *J. Geophys. Res.*, *106*, 7–22.

Kangas, J., A. Aikio, and J. V. Olson (1986), Multistation correlation of ULF pulsation spectra associated with sudden impulses, *Planet. Space Sci.*, *34*, 543–553.

Kennel, C. F., and H. E. Petschek (1966), Limit on stably trapped particle fluxes, *J. Geophys. Res.*, *71*, 1–28.

Kerttula, R., K. Mursula, T. Pikkarainen, and J. Kangas (2001a), Storm-time Pc1 activity at high and middle latitudes, *J. Geophys. Res.*, *106*, 6213–6227.

Kerttula, R., K. Mursula, T. Pikkarainen, and J. Kangas (2001b), Effect of magnetic storm intensity on Pc1 activity at high and middle latitudes, *J. Atmos. Sol. Terr. Phys.*, *63*, 503–511.

Khazanov, G. V., K. V. Gamayunov, D. L. Gallagher, and J. U. Kozyra (2006), Self-consistent model of magnetospheric ring current and propagating electromagnetic ion cyclotron waves: Waves in multi-ion magnetosphere, *J. Geophys. Res.*, *111*, A10202, doi:10.1029/2006JA011833.

Kozyra, J. U., V. K. Jordanova, R. B. Horne, and R. M. Thorne (1997), Modeling of the contribution of electromagnetic ion cyclotron (EMIC) waves to stormtime ring current erosion, in *Magnetic Storms*, *Geophys. Monogr. Ser.*, vol. 98, edited by B. Tsurutani et al., pp. 187–202, AGU, Washington, D. C.

Lyons, L. R., R. M. Thorne, and C. F. Kennel (1972), Pitch-angle diffusion of radiation belt electrons within the plasmasphere, *J. Geophys. Res.*, *77*, 3455–3474.

Manchester, R. N. (1966), Propagation of Pc1 micropulsations from high to low latitudes, *J. Geophys. Res.*, *71*, 3749–3754.

Manchester, R. N., and B. J. Fraser (1970), Occurrence of hydromagnetic emissions at two southern hemisphere sites, *Planet. Space Sci.*, *18*, 291–297.

Meredith, N. P., R. M. Thorne, R. B. Horne, D. Summers, B. J. Fraser, and R. R. Anderson (2003), Statistical analysis of relativistic electron energies for cyclotron resonance with EMIC waves observed on CRRES, *J. Geophys. Res.*, *108*(A6), 1250, doi:10.1029/2002JA009700.

Moldwin, M. B., J. Howard, J. Sanny, J. D. Bocchicchio, H. K. Rassoul, and R. R. Anderson (2004), Plasmaspheric plumes: CRRES observations of enhanced density beyond the plasmapause, *J. Geophys. Res.*, *109*, A05202, doi:10.1029/2003JA010320.

O'Brien, T. P., and M. B. Moldwin (2003), Empirical plasmapause models from magnetic indices, *Geophys. Res. Lett.*, *30*(4), 1152, doi:10.1029/2002GL016007.

Olson, J. V., and L. C. Lee (1983), Pc1 wave generation by sudden impulses, *Planet. Space Sci.*, *31*, 295–302.

Perraut, S., R. Gendrin, A. Roux, and C. de Villedary (1984), Ion cyclotron waves: Direct comparison between ground-based measurements and observations in the source region, *J. Geophys. Res.*, *89*, 195–202.

Rauch, J. L., and A. Roux (1982), Ray tracing of ULF waves in a multicomponent magnetospheric plasma: Consequences for the generation mechanism of ion cyclotron waves, *J. Geophys. Res.*, *87*, 8191–8198.

Smith, A. J., R. B. Horne, and N. P. Meredith (2004), Ground observations of chorus following geomagnetic storms, *J. Geophys. Res.*, *109*, A02205, doi:10.1029/2003JA010204.

Søraas, F., J. A. Lundblad, N. F. Maltseva, V. Troitskaya, and V. Selivanov (1980), A comparison between simultaneous I.P.D.P. ground-based

observations and observations of energetic protons obtained by satellites, *Planet. Space Sci.*, *28*, 387–405.

Søraas, F., K. Aarsnes, J. A. Lundblad, and D. S. Evans (1999), Enhanced pitch angle scattering of protons at mid-latitudes during geomagnetic storms, *Phys. Chem. Earth Part C*, *24*, 287–292.

Spasojević, M., H. U. Frey, M. F. Thomsen, S. A. Fuselier, B. R. Sandel, and U. S. Inan (2004), The link between a detached subauroral proton arc and a plasmaspheric plume, *Geophys. Res. Lett.*, *31*, L04803, doi:10.1029/2003GL018389.

Summers, D., and R. M. Thorne (2003), Relativistic electron pitch-angle scattering by electromagnetic ion cyclotron waves during geomagnetic storms, *J. Geophys. Res.*, *108*(A4), 1143, doi:10.1029/2002JA009489.

Takahashi, K., B. J. Anderson, and R. J. Strangeway (1990), AMPTE CCE observations of Pc 3–4 pulsations at L = 2–6, *J. Geophys. Res.*, *95*, 17,179–17,186.

Taylor, W. W. L., B. K. Parady, P. B. Lewis, R. L. Arnoldy, and L. J. Cahill Jr. (1975), Initial results from the search coil magnetometer at Siple, Antarctica, *J. Geophys. Res.*, *80*, 4762–4769.

Tepley, L., and R. K. Landshoff (1966), Waveguide theory for ionospheric propagation of hydromagnetic emissions, *J. Geophys. Res.*, *71*, 1499–1504.

Thorne, R. M., E. J. Smith, R. K. Burton, and R. E. Holzer (1973), Plasmaspheric hiss, *J. Geophys. Res.*, *78*, 1581–1596.

Thorne, R. M., R. B. Horne, S. Glauert, N. P. Meredith, Y. Y. Shprits, D. Summers, and R. R. Anderson (2005), The influence of wave-particle interactions on relativistic electron dynamics during storms, in *Inner Magnetosphere Interactions: New Perspectives From Imaging*, *Geophys. Monogr. Ser.*, vol. 159, edited by J. Burch, M. Schulz, and H. Spence, pp. 101–112, AGU, Washington, D. C.

Tsyganenko, N. A. (1996), Effects of the solar wind conditions on the global magnetospheric configuration as deduced from data-based field models, in *Proceedings of the Third International Conference on Substorms (ICS-3)*, edited by E. J. Rolfe and B. Kaldeich-Schürmann, *Eur. Space Agency Spec. Publ.*, *ESA-SP-389*, 191–186.

Wentworth, R. C. (1964), Enhancement of hydromagnetic emissions after geomagnetic storms, *J. Geophys. Res.*, *69*, 2291–2298.

Yahnina, T. A., A. G. Yahnin, J. Kangas, J. Manninen, D. S. Evans, A. G. Demekhov, V. Y. Trakhtengerts, M. F. Thomsen, G. D. Reeves, and B. B. Gvozdevsky (2003), Energetic particle counterparts for geomagnetic pulsations of Pc1 and IPDP types, *Ann. Geophys.*, *21*, 2281–2292.

J. Bortnik, Department of Atmospheric and Oceanic Sciences, University of California, Los Angeles, CA 90095-1565, USA. (jbortnik@gmail.com)

D. Detrick, Institute for Physical Science and Technology, University of Maryland, College Park, MD 20742-2431, USA. (detrick@umd.edu)

M. Engebretson and J. Posch, Department of Physics, Augsburg College, Minneapolis, MN 55454-1331, USA. (engebret@augsburg.edu; posch@augsburg.edu)

J. C. Green, NOAA Space Environment Center, Boulder, CO 80305, USA. (janet.green@noaa.gov)

R. B. Horne and M. C. Rose, British Antarctic Survey, High Cross, Madingley Road, Cambridge, CB3 OET, U.K. (rh@bas.ac.uk; mcr@bas.ac.uk)

M. Lessard, Space Science Center, University of New Hampshire, Durham, NH 03824, USA. (marc.lessard@unh.edu)

J. Manninen, Sodankylä Geophysical Observatory, Tähteläntie 62, FIN-99600 Sodankylä, Finland. (jyrki.manninen@sgo.fi)

N. Petit, Department of Computer Science, Augsburg College, Minneapolis, MN 55454-1331, USA. (petit@augsburg.edu)

A. Weatherwax, Department of Physics, Siena College, Loudonville, NY 12211-1462, USA. (aweatherwax@siena.edu)